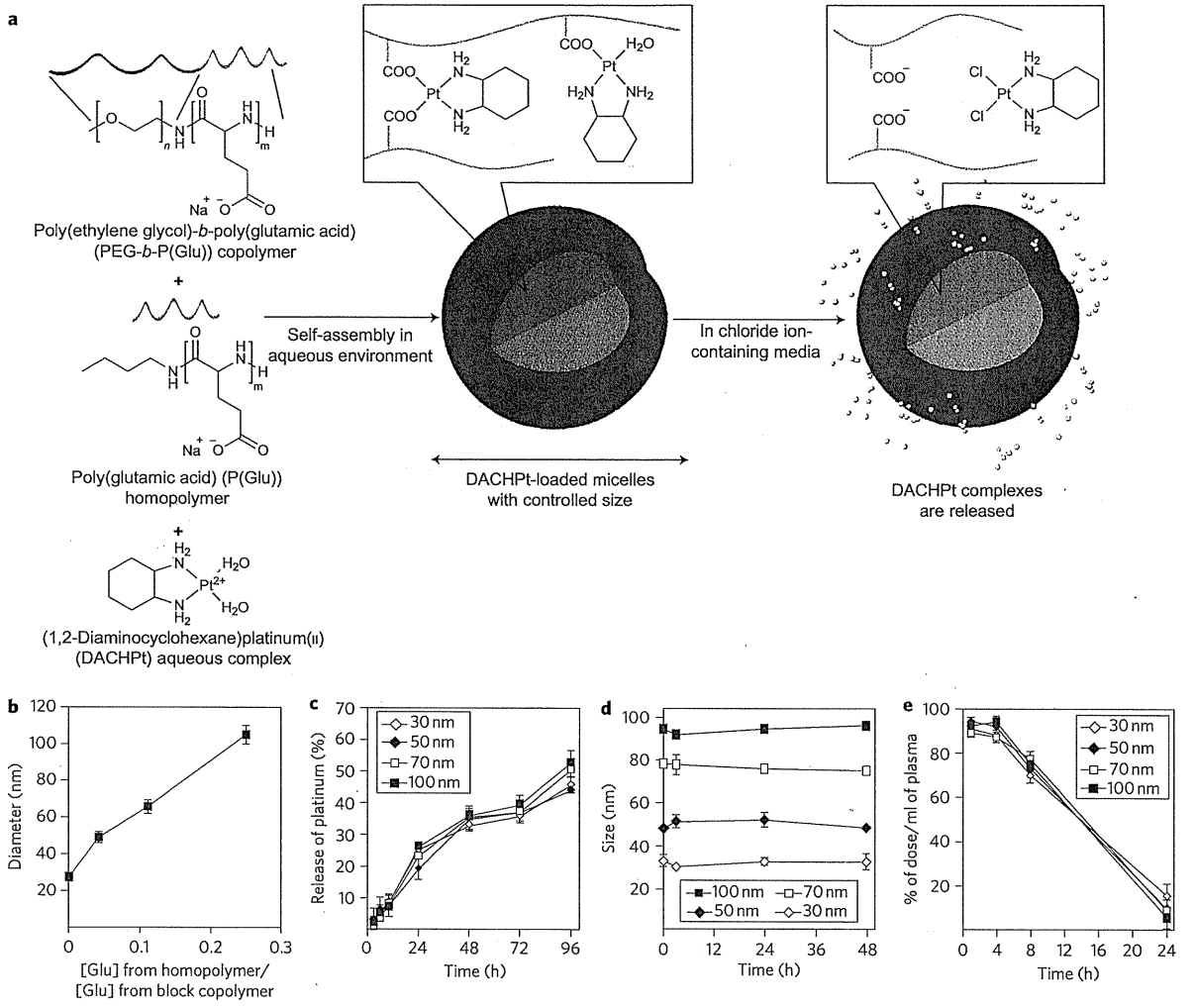

Figure 1 | Construction and physicochemical properties of DACHPt-loaded micellar nanomedicines (DACHPt/m) with different diameters. a, Schematic showing DACHPt/m formed through the interaction between DACHPt and the carboxylic groups of poly(glutamic acid) (green) in PEG-*b*-P(Glu) and P(Glu). In media containing chloride ions, DACHPt (yellow circles) is released from the micelles through ligand exchange between the carboxylic groups in P(Glu) and the chloride ions. **b**, Changing micelle size by altering the ratio of P(Glu) from the homopolymer and the P(Glu) portion of PEG-*b*-P(Glu) in the mixture. Total glutamic acid residue concentration was maintained at 5 mM. **c**, Micelles of all sizes release DACHPt at similar rates. **d**, Micelles of all sizes incubated in cell culture media containing 10% serum at 37 °C maintained their sizes over 48 h. **e**, Plasma clearances of micelles with different diameters follow similar trends. Data are means ± s.e.m., $n = 3$.

Table 1 | Diameter, size distribution, drug loading and surface charge of 30, 50, 70 and 100 nm micelles.

Size (nm)*	Polydispersity index	[Pt]/[COO] (mol/mol)†	Pt/polymer (wt/wt%)	Zeta-potential (mV)‡
30	0.16	0.56	34	−2.29 ± 1.41
54	0.14	0.6	48	−1.61 ± 0.58
69	0.12	0.57	54	−0.89 ± 0.33
110	0.11	0.52	69	0.15 ± 0.21

*Determined by DLS. †Determined by ICP-MS (platinum concentration) and weight of micelles. ‡Determined by laser doppler electrophoresis ($n = 4$, mean ± s.d.).

The 30, 50, 70 and 100 nm DACHPt/m presented similar zeta potentials, ranging from −2.29 to 0.15 mV at pH 7.4 (Table 1). These micelles showed similar drug release rates (Fig. 1c), driven by the ligand exchange of DACHPt between the carboxylic groups of P(Glu) and the chloride ions in the biological media. After 96 h incubation in cell culture media containing 10% fetal bovine serum (FBS) at 37 °C, the drug release from DACHPt/m reached ~50% (Fig. 1c). Under similar conditions, differently sized DACHPt/m maintained their diameters for over 48 h (Fig. 1d). DACHPt/m of different sizes also showed similar plasma clearance rates (~12% of injected dose (ID) per ml plasma remained after 24 h) and plasma half-lives (7–8 h) (Fig. 1e and Supplementary Table S1, respectively). We recently showed that DACHPt/m can maintain their micellar structure in the circulation for at least 24 h after injection[28]. Furthermore, DACHPt/m of varying sizes show similar distributions in the kidney, liver and spleen (Supplementary Fig. S2 and

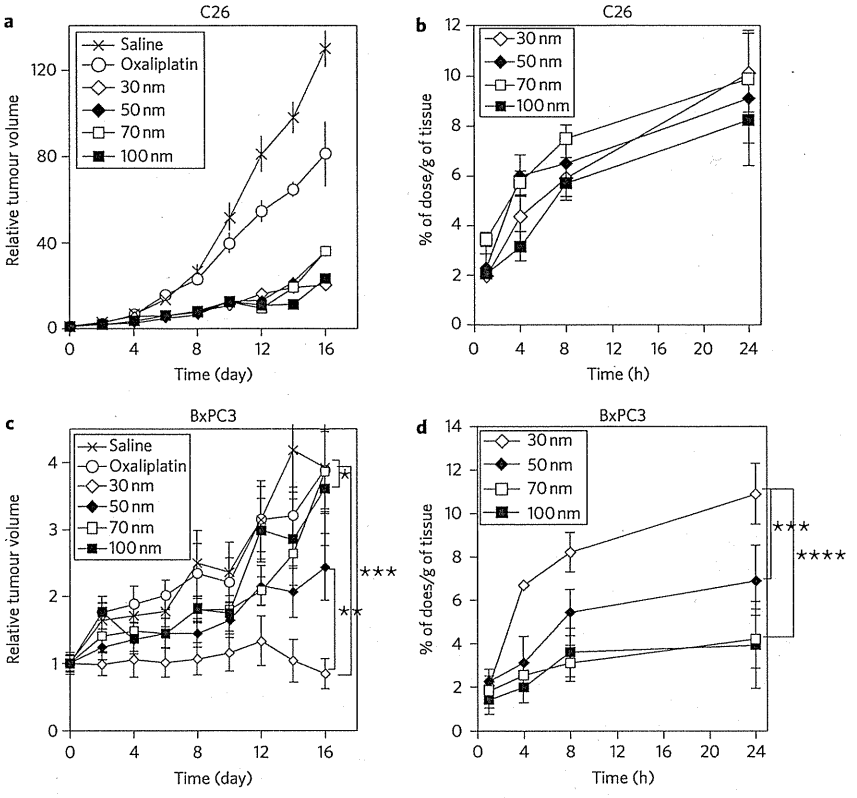

Figure 2 | Anticancer activity and tumour accumulation of DACHPt/m with different diameters. a–d, Plots of relative tumour volumes of subcutaneous hyperpermeable murine colon adenocarcinoma (C26) (**a**) and subcutaneous hypopermeable human pancreatic adenocarcinoma BxPC3 (**c**) tumours, and accumulation of DACHPt/m in C26 (**b**) and BxPC3 (**d**) tumours. To evaluate antitumour activity, oxaliplatin was injected on days 0, 2 and 4 (dose, 8 mg kg^{-1}) and micelles were injected on days 0, 2 and 4 (dose, 3 mg kg^{-1} on a platinum basis). For tumour accumulation experiments, micelles were injected at 100 μg per mouse on a platinum basis. Data are means ± s.e.m., $n = 6$. *$P > 0.05$; **$P < 0.05$; ***$P < 0.01$; ****$P < 0.001$.

Table S1), which are the major organs responsible for the clearance of nanocarriers[29]. The levels of accumulation of DACHPt/m in these organs are comparable to other polymeric micelles incorporating cisplatin[8] or doxorubicin[9], except for a slightly higher accumulation of 100 nm DACHPt/m in the liver. Because the surface chemistry and charge of nanocarriers have been reported to critically affect the interactions of nanocarriers with plasma proteins and cells and the biodistributions of nanocarriers[21,22,29,30], the analogous surface chemistry (PEG-coated surface), neutral charge and comparable plasma clearance of DACHPt/m with different diameters are substantial advantages for the evaluation of their extravasation, penetration and accumulation abilities in solid tumours as well as the associated therapeutic outcomes.

Antitumour activity of DACHPt/m in solid tumours

The antitumour activity and accumulation of DACHPt/m with different diameters were examined in tumour models with different permeabilities: a hyperpermeable murine colon adenocarcinoma 26 (C26) model characterized by high vascularization and slight tumour stroma[31] and a human pancreatic adenocarcinoma BxPC3 characterized by low vascularization, reduced vascular permeability due to pericyte coverage of blood vessels[20,31] and thick fibrosis, which are representative characteristics of some intractable solid tumours[20,31–33]. Note that the *in vitro* cytotoxicity of sub-100 nm DACHPt/m on C26 and BxPC3 cell lines was not substantially affected by micelle size (Supplementary Table S3), suggesting that their *in vivo* antitumour effect can be associated with their accumulation and microdistribution in solid tumours. In the C26 model, all micelles demonstrated comparable tumour growth inhibition (Fig. 2a), whereas oxaliplatin did not show a significant antitumour effect. The accumulation levels of all sub-100 nm micelles in C26 tumours were consistently comparable, reaching ~10% ID g^{-1} tumour at 24 h post-injection (Fig. 2b). In the BxPC3 model, the size effect of DACHPt/m on antitumour activity became evident, with the 30 nm micelles completely suppressing tumour growth, the 50 nm micelles leading to reduced antitumour activity, and the 70 nm and 100 nm micelles failing to show any antitumour effect (Fig. 2c). The accumulation of the 30 nm micelles was two times higher than that of the 50 nm micelles and four times higher than that of the 70 and 100 nm micelles after 24 h in BxPC3 tumours (Fig. 2d), which is also consistent with the antitumour efficacies in Fig. 2c.

The intratumoral microdistribution of fluorescently labelled DACHPt/m with different sizes in tumour sections was studied to investigate size-dependent extravasation and penetration of micellar nanomedicines in tumours. Histological investigations using haematoxylyn and eosin (H&E) staining revealed a well-vascularized medullary histological pattern of C26 tumours with reduced tumour stroma (Fig. 3a). In this tumour model, the fluorescence signals from the 30, 50, 70 and 100 nm micelles were uniformly distributed throughout the entire section at 24 h post-injection, suggesting deep tumour penetration of all sub-100 nm micelles (Fig. 3b, red). The immunofluorescence localization of platelet endothelial cell adhesion molecule-1 (PECAM-1), expressed by endothelial cells, indicated the extensive distribution of blood vessels in C26 tumours (Fig. 3b, green). However, H&E staining of BxPC3 tumours revealed the formation of nests of cancer cells surrounded by fibrotic tissue (Fig. 3c), which may act as a barrier

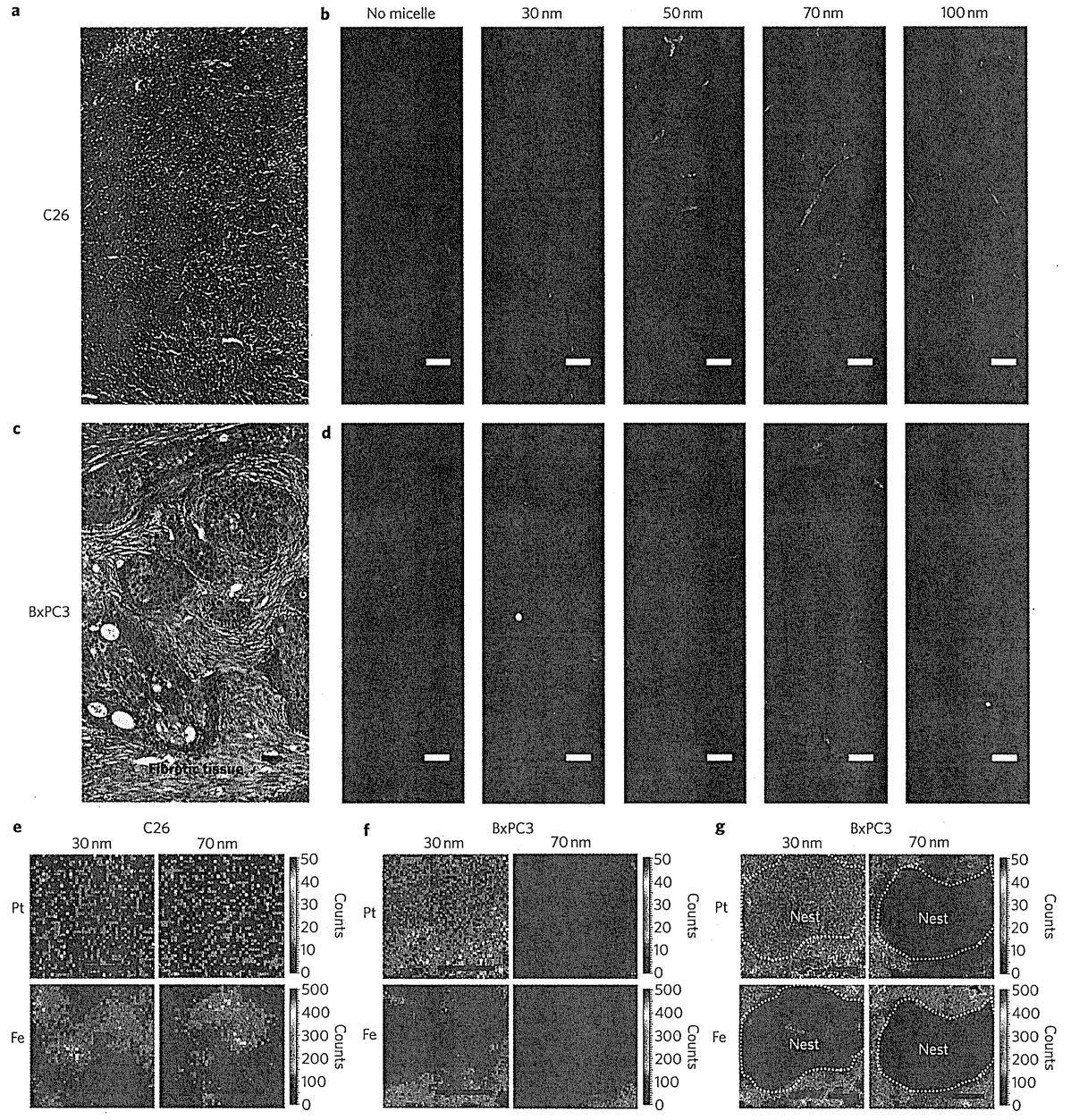

Figure 3 | Microdistribution of fluorescently labelled DACHPt/m of varying sizes in tumours. a–d, Histological examination of C26 tumour (**a**) and BxPC3 tumour (**c**) by H&E staining (dashed lines in **c** show area of cancer cell nests in the BxPC3 tumour) and fluorescent microscopic images of sections of C26 (**b**) and BxPC3 (**d**) tumours 24 h after intravenous administration of fluorescent micelles with different sizes. Micelles were labelled with Alexa 594 (red). Blood vessels were marked with PECAM-1 and Alexa 488 secondary antibody (green). Scale bars, 50 μm. **e–g**, Mapping of platinum atoms from DACHPt and iron from haemoproteins in tumour sections of C26 (**e**), BxPC3 (**f**) and a BxPC3 cancer cell nest (indicated by dashed line) (**g**) by μ-SR-XRF 24 h after administration of micelles. Scale bars, 50 μm.

against the penetration of drugs and nanocarriers[20,31]. In the BxPC3 model, immunofluorescence detection of PECAM-1 (Fig. 3d, green) indicated the presence of blood vessels around the cancer cell nests and the absence of vessels in the interior of these structures. We observed that the 30 nm micelles penetrated inside the tightly nested structures of BxPC3 tumours, but the fluorescent signal of the bigger micelles diminished and was concentrated close to the blood vessels, indicating their failure to enter the nests of cancer cells (Fig. 3d, red). This size-dependent penetration of fluorescent DACHPt/m may affect the intratumoral distribution of the delivered drug.

Given that the drug loaded in the micelles was a platinum complex, we assessed the drug microdistribution in tumour sections by detecting element disposition using μ-synchrotron radiation X-ray fluorescence (μ-SR-XRF). The very distinct peak of the platinum from the DACHPt can be observed in the sum spectrum of the line scan as well as the elements traditionally present in animal tissue. The distribution of iron and platinum in tumour tissue

sections was studied to evaluate the distribution of haemoproteins (linked to the presence of blood vessels) and the location of the drug, respectively. For this experiment, we used DACHPt/m with diameters of 30 and 70 nm because of the critical differences in antitumour activity, tumour accumulation and microdistribution of DACHPt/m in the BxPC3 tumour model for diameters below and above 50 nm (Figs 2c,d, 3d).

In the C26 tumour model, the extensive spread of iron atoms indicates abundant vascularization (Fig. 3e), consistent with the abundance of blood vessels observed by immunofluorescence microscopy (Fig. 3b, green). DACHPt delivered from the 30 and 70 nm micelles was broadly distributed in this tumour model (Fig. 3e). In the BxPC3 xenografts, the distribution of iron atoms (Fig. 3f,g) indicates reduced vascularization and disposition of blood vessels in this model, suggesting a restricted blood flow inside the nest structures. The platinum mapping shows that the 30 nm micelles delivered DACHPt inside the cancer cell nests, whereas DACHPt from the 70 nm micelles is localized in the periphery of the nests (Fig. 3g). In both tumour models, the intratumoral microdistribution of DACHPt has a layout similar to that of the fluorescent micelles, confirming that tumour penetration by the micelles directly affects drug accumulation and antitumour outcome.

The real-time observation of *in vivo* behaviour of nanocarriers might reveal the critical barriers in a living body. Unlike conventional histological analysis, the *in vivo* confocal laser scanning microscopy (CLSM) technique enables spatiotemporal and quantitative analyses of extravasation, tissue penetration and cellular internalization of nanocarriers in a living animal[34]. By using an *in vivo* CLSM combined with a high-speed resonance scanner designed to acquire clean live tissue images, we intravitally evaluated the penetration and accumulation of the fluorescently labelled micelles. The 30 and 70 nm micelles were labelled with Alexa 488 (green) and Alexa 594 (red) fluorescent probes, respectively (Supplementary Fig. S3), and concurrently injected into tumour-bearing mice to evaluate real-time extravasation, penetration and microdistribution of both micelles in the same tumour (Fig. 4). Fluorescence measurements in the tissues were relative to the fluorescence intensity in the vasculature immediately after injection of the micelles (V_{max}).

At 1 h post-injection of the micelles, the fluorescence intensity of both 30 and 70 nm DACHPt/m in the blood vessels of tumours was ~80% of V_{max} (Fig. 4a,b). In C26 tumours, the micelles showed similar extravasation and penetration (Fig. 4a, Supplementary Video S1). The z-stack volume reconstruction of the C26 tumour showed a profusely vascularized structure and a comparable presence of both micelles in the tumour interstitium (Fig. 4c, Supplementary Video S2). In BxPC3 tumours, the extravasation profiles of the 30 and 70 nm micelles after 1 h were clearly dissimilar (Fig. 4b, Supplementary Videos S3, S4). The 30 nm micelles crossed the vascular wall, achieving over 20% of V_{max} at 40 μm from the blood vessel (Fig. 4b). In contrast, the 70 nm micelles extravasated at discrete sites close to the blood vessels and failed to move towards the interstitial space (Fig. 4b). These distinct penetration profiles were evident in the z-stack volume reconstruction of the BxPC3 tumour, showing that the extravasation points of the 70 nm micelles surrounded the blood vessels (Fig. 4d,e, Supplementary Videos S5 and S6). At 24 h post-injection, the intensities of the extravasated 30 and 70 nm micelles in the C26 tumour were ~40% of V_{max} at 100 μm from the blood vessels (Fig. 4f), and both micelles were observed inside the individual cells of the tumour tissue (Fig. 4f). In BxPC3 tumours, the distribution of the micelles corresponded reasonably to their different extravasation profiles; the 30 nm micelles achieved deep tumour accumulation, but the 70 nm micelles remained close to the vasculature (Fig. 4g, white arrows). The intensity of the extravasated 30 nm micelles was ~40% of V_{max} (Fig. 4g) and they apparently localized in the cells (Fig. 4g). These observations strongly suggest that 30 nm DACHPt/m can penetrate nests of cancer cells distant from blood vessels, allowing homogeneous drug distribution in hypopermeable tumours.

Although many factors (including morphology, hydrophobicity and nanoparticle charge) affect their accumulation in tumours, it is of primary importance to study long-circulating nanocarriers, because prolonged circulation is a prerequisite for tumour targeting based on the EPR effect. Results obtained by intratumoral microdistribution studies indicate that micellar nanomedicines with diameters less than 50 nm might be superior in terms of extravasation and penetration into tumour tissues among the sub-100 nm micellar nanomedicines. The limitation of the present study is that the size of the micellar nanomedicines was restricted to between 30 and 100 nm. Because the threshold of renal clearance of nanoparticles is ~5.5 nm (ref. 35), tumour accumulation and intratumoral distribution of nanomedicines in the range between 5 and 30 nm remain to be clarified. Furthermore, the biodistribution study revealed that the 100 nm micelles showed higher accumulation in the liver compared with other smaller micelles (Supplementary Fig. S2, Table S1), suggesting the importance of the size of nanomedicines for their distribution in organs, which may be associated with toxicity. Hence, optimizing the size of nanomedicines should take into account the balance between antitumour efficacy and potential toxicity.

Enhancing tumour permeability with a TGF-β inhibitor

We have recently reported that low doses of a transforming growth factor (TGF)-β inhibitor (TGF-β-I) transiently decreases the pericyte coverage of the endothelium in the neovasculature of pancreatic tumours, resulting in enhanced accumulation and antitumour activity of 65 nm micellar nanomedicines and 90 nm Doxil[20]. These results motivated us to evaluate the effect of the TGF-β inhibitor on the delivery of sub-100 nm DACHPt/m in BxPC3 tumours. When mice were treated with 1 mg kg^{-1} of TGF-β-I (LY364947), the 70 nm micelles reduced the tumour growth rate as effectively as the 30 nm micelles (Fig. 5a). Moreover, accumulation of the 70 nm micelles in tumours was augmented to a level comparable with that of the 30 nm micelles (Fig. 5b). These results indicate that the impaired extravasation and penetration of the 70 nm micelles in BxPC3 tumours can be overcome by treatment with TGF-β-I.

Fluorescence microscopic evaluation of BxPC3 tumour sections revealed that the fluorescently labelled 70 nm micelles showed enhanced intratumoural penetration even inside cancer cell nests after administration of TGF-β-I (Fig. 5c). This result suggests that modulation of the stromal components in tumour tissue by TGF-β-I, including pericyte coverage around the tumour blood vessels, is important for penetration of the 70 nm micelles. Moreover, the μ-SR-XRF measurement demonstrated that co-administration of TGF-β-I facilitated intratumoral delivery of DACHPt from the 70 nm micelles, which reached the interior of the cancer cell nests at 24 h post-injection (Fig. 5d). This result is consistent with the augmented antitumour activity (Fig. 5a) and enhanced intratumoural penetration (Fig. 5b) of 70 nm DACHPt/m by TGF-β-I.

Intravital CLSM observation also confirmed that treatment with TGF-β-I enhanced the extravasation and penetration of 70 nm micelles into BxPC3 tumours (Fig. 5e, Supplementary Video S7). We found that the 30 and 70 nm micelles demonstrated a comparable distribution in the tumour tissues, and both achieved ~20% of V_{max} at 40 μm from the blood vessels at 1 h after co-injection (Fig. 5e). At 24 h after injection, both micelles had deeply penetrated the tumour (Fig. 5f), reaching over 40% of V_{max} at 100 μm from the blood vessels (Fig. 5f). The 30 and 70 nm micelles also appeared to show comparable subcellular localization (Fig. 5f). These results suggest that the improvement in extravasation and penetration of 70 nm DACHPt/m by TGF-β-I caused the increased antitumour

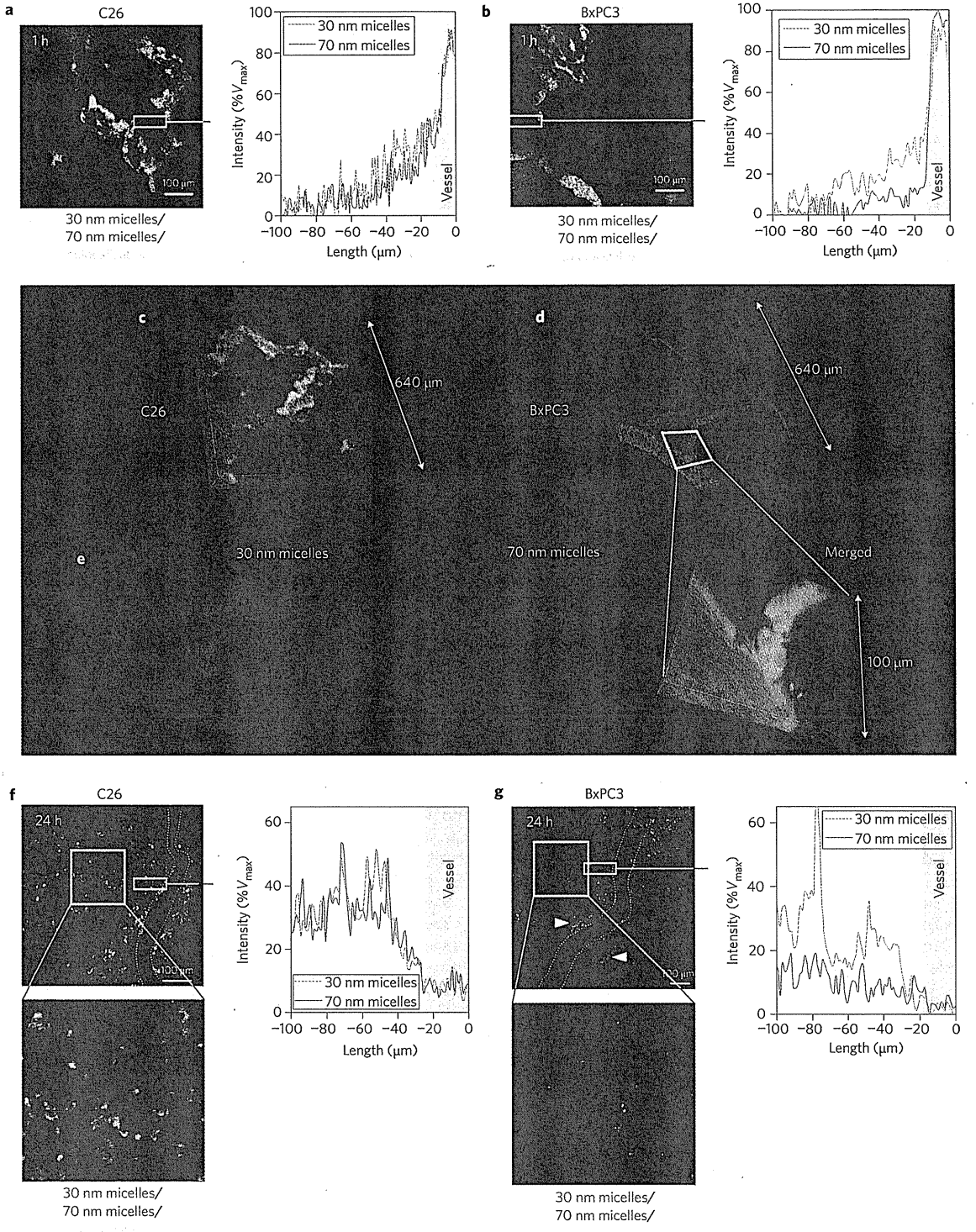

Figure 4 | *In vivo* real-time microdistribution of DACHPt/m with different diameters in tumours. a,b, Microdistribution of fluorescently labelled 30 nm (green) and 70 nm (red) micelles 1 h after injection into C26 (**a**) and BxPC3 (**b**) tumours. Their colocalization is shown in yellow. Right panels in **a** and **b** show fluorescence intensity profile from the blood vessel (0–10 μm; grey area) to the tumour tissue (10–100 μm) in the selected region (indicated by a white rectangle) expressed as a percentage of the maximum fluorescence intensity attained in the vascular region (%V_{max}). **c,d**, Z-stack volume reconstruction of C26 (**c**) and BxPC3 (**d**) tumours 1 h after co-injection of the fluorescent micelles. **e**, Magnification of the perivascular region (indicated by a white trapezium) of the z-stack volume image of BxPC3 tumours. **f,g**, Distribution of 30 and 70 nm micelles 24 h after injection into C26 tumours (**f**) and BxPC3 tumours (**g**). White arrows in **g** indicate 70 nm micelles localizing at perivascular regions. Right panels show fluorescence intensity profile from the blood vessel (0–10 μm; grey area) to the tumour tissue (10–100 μm) in the selected region (indicated by white rectangle).

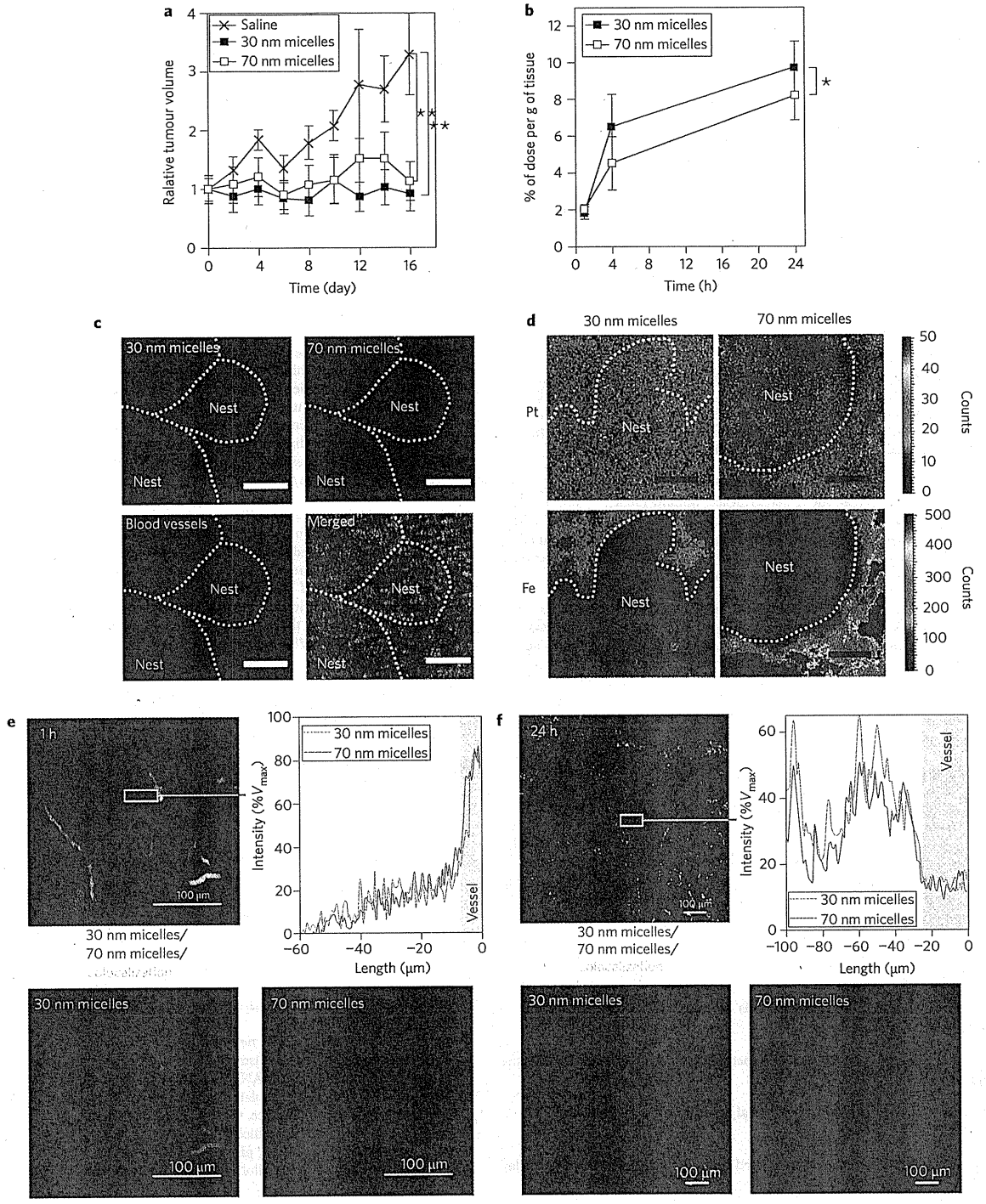

Figure 5 | Effect of TGF-β inhibitor (TGF-β-I) on antitumour activity and tumour accumulation of DACHPt/m in BxPC3 tumours. a, Graph showing relative tumour volume. Micelles (3 mg kg^{-1}) were injected on days 0, 4 and 8 and TGF-β-I on days 0, 2, 4, 6 and 8. **b**, Graph showing accumulation of 30 and 70 nm DACHPt/m in BxPC3 tumours after injection of TGF-β-I. Data are expressed as means ± s.e.m., $n = 6$. *$P > 0.05$; **$P < 0.01$. **c**, Fluorescent microscopy of tumour sections 24 h after co-administration of the fluorescent micelles and TGF-β-I. Scale bars, 50 μm. **d**, Platinum and iron mapping of tumour sections by μ-SR-XRF 24 h after administration of 30 and 70 nm micelles. Scale bars, 50 μm. **e**,**f**, Intravital distribution of 30 nm (green) and 70 nm (red) micelles in BxPC3 tumours 1 h (**e**) and 24 h (**f**) after co-injection of micelles and TGF-β-I. Their colocalization is shown in yellow. Right panels show fluorescence intensity profile from the blood vessel (grey area) to the tumour tissue in the selected region (indicated by a white rectangle).

activity, supporting the hypothesis that TGF-β inhibitors have great potential for enhancing the therapeutic efficacy of nanomedicines in hypopermeable tumours.

Conclusions

The enhanced targeting of drugs to cancer cells within tumours by nanomedicines largely depends on size. We have shown that the

tumoricidal efficiency of long-circulating polymeric micelles depends on the size of the micelles and the permeability of the tumour. In hypervascular tumours with a highly permeable structure, sub-100 nm micellar nanomedicines showed no size-dependent restrictions on extravasation and penetration in tumours. In contrast, only nanomedicines smaller than 50 nm can penetrate poorly permeable hypovascular tumours. Furthermore, increasing the permeability of hypovascular tumours using TGF-β signalling inhibitor improved the accumulation and distribution of the larger 70 nm micelles, offering a way to enhance the efficacy of larger nanomedicines. Because efficient extravasation and tumour penetration are important prerequisites for targeting cancer cells, our findings are important for designing sophisticated nanomedicines that are capable of cell recognition and selective intracellular release of payloads.

Materials and methods

Materials, cell lines and animals. Information regarding materials, cell lines (murine colon adenocarcinoma 26 (C26) cells and human pancreatic cancer BxPC3 cells) and animals is described in the Supplementary Information. All animal experiments were performed in accordance with the Guidelines for the Care and Use of Laboratory Animals as stated by the University of Tokyo.

Tumour models. BALB/c nude mice were inoculated subcutaneously with C26 cells (1×10^6 cell ml^{-1}) to prepare the hyperpermeable tumour model, or with BxPC3 cells (1×10^7 cell ml^{-1}) to prepare the hypopermeable tumour model. *In vivo* and *ex vivo* confocal microscopy, elemental mapping and antitumour activity studies were performed when tumours were 50 mm in volume[3]. Biodistribution studies were performed when the tumours were ~100 mm in volume[3].

Preparation of PEG-*b*-P(Glu) block copolymer and P(Glu) homopolymer. PEG-*b*-P(Glu) block copolymers and P(Glu) homopolymers were synthesized according to a previously described synthetic method[8] with a minor modification. Detailed procedures for polymer synthesis and characterization are described in the Supplementary Information. PEG-*b*-P(Glu) was fluorescently labelled by conjugating the Alexa 488 and Alexa 594 succinimidyl esters to the ω-amino group of the polymer in dimethyl sulfoxide. Detailed procedures are described in the Supplementary Information.

Preparation and characterization of DACHPt/m with different diameters. DACHPt/m with different diameters were prepared according to a previously described method with a slight modification[10,26,27]. Detailed procedures are described in the Supplementary Information. The size distribution of DACHPt/m was evaluated by DLS measurements at 25 °C, and the zeta potential of the micelles was measured in phosphate buffer at pH 7.4 using a Zetasizer Nano ZS90 (Malvern Instruments). The platinum content in the micelles was determined by ion-coupled plasma-mass spectrometry (ICP-MS) using a Hewlett Packard 4500 ICP-MS. Fluorescently labelled DACHPt/m was prepared in a similar manner with Alexa 488 or Alexa 594 labelled PEG-*b*-P(Glu). The stability of DACHPt/m with different diameters in Dulbecco's modified Eagle's medium (DMEM) containing 10% FBS at 37 °C was determined by DLS. The release rate of the micelles under similar conditions was studied by the dialysis method using a dialysis bag (molecular weight cutoff = 2,000). More detailed information is described in the Supplementary Information.

Transmission electron microscopy. The experimental procedure is described in the Supplementary Information.

***In vitro* cytotoxicity assay.** The experimental procedure is described in the Supplementary Information.

Antitumour activity assay. Mice were treated three times intravenously at two-day intervals with 3 mg kg^{-1} (on a platinum basis) of 30, 50, 70 and 100 nm DACHPt/m. Anti-tumour activity was evaluated in terms of tumour size (V), which was estimated by the equation

$$V = a \times b^2/2$$

where a and b are the major and minor axes of the tumour, respectively, as measured by a caliper. The statistical significance of different findings between the experimental and control groups was determined by analysis of variance (ANOVA) with Tukey's multiple comparison test. The results were considered statistically significant if two-tailed P-values were less than 0.05.

Plasma clearance and organ and tumour accumulation of DACHPt/m with different diameters. The experimental procedure is described in the Supplementary Information.

Microdistribution and immunohistochemistry of fluorescently labelled DACHPt/m. Mice bearing C26 or BxPC3 tumours were intravenously injected with Alexa 594-labelled 30, 50, 70 and 100 nm DACHPt/m at 100 μg per mouse on a platinum basis. Twenty-four hours later, tumours were collected and immediately frozen in an acetone/dry ice mixture. The frozen samples were further sectioned (thickness, 16 μm) in a cryostat, briefly fixed with cold acetone and then incubated with PECAM-1 antibody. Alexa 488 was used as the secondary antibody. Samples were observed using a Zeiss LSM510 Meta confocal microscope (Oberkochen). For H&E staining, the excised samples were fixed overnight in 4% paraformaldehyde and then paraffin-embedded to prepare them for the perfusion study in the tumour tissues. Samples were observed under an AX80 microscope (Olympus).

Element array analysis using μ-X-ray fluorescence. SR-XRF was used to determine DACHPt as well as iron distribution in sections of solid tumours (C26 or BxPC3) at 24 h post-intravenous injection of 30 and 70 nm DACHPt/m[36]. The detailed experimental procedure is described in the Supplementary Information.

***In vivo* confocal laser scanning microscopy (*in vivo* CLSM).** Mice bearing C26 or BxPC3 tumours were intravenously co-injected with fluorescently labelled 30 and 70 nm DACHPt/m at a dose of 10 mg kg^{-1}. The 30 nm micelles were labelled with Alexa 488, and the 70 nm micelles were labelled with Alexa 594. The *in vivo* CLSM observation of tumour tissues was performed according to a previously reported method[28,34]. All *in vivo* picture acquisitions were performed using a Nikon A1R confocal laser scanning microscope system attached to an upright ECLIPSE FN1 (Nikon). The 30-nm-diameter micelles were detected using 488/510 nm excitation/emission filters, and the signal from the 70 nm micelles was acquired with 560/620 nm excitation/emission filters.

Enhancement of tumour permeability by treatment with a TGF-β inhibitor. The effect of TGF-β inhibitor on the accumulation and antitumour activity of DACHPt/m was determined using the methods already described. For the antitumour activity experiment, BxPC3-bearing mice were administered intraperitoneal injections of TGF-β inhibitor LY364947 at 1 mg kg^{-1} every second day. For tumour accumulation studies, BxPC3-bearing mice received an intraperitoneal injection of the TGF-β inhibitor at 1 mg kg^{-1} at 1 h before co-injection of the 30 and 70 nm micelles.

Received 27 April 2011; accepted 12 September 2011; published online 23 October 2011

References

1. Duncan, R. The dawning era of polymer therapeutics. *Nature Rev. Drug Discov.* **2,** 347–360 (2003).
2. Ferrari, M. Cancer nanotechnology: opportunities and challenges. *Nature Rev. Cancer.* **5,** 161–171 (2005).
3. Torchilin, V. P. Recent advances with liposomes as pharmaceutical carriers. *Nature Rev. Drug Discov.* **4,** 145–160 (2005).
4. Davis, M. E., Chen, Z. & Shin, D. Nanoparticle therapeutics: an emerging treatment modality for cancer. *Nature Rev. Drug Discov.* **7,** 771–782 (2008).
5. Kataoka, K., Harada, A. & Nagasaki, Y. Block copolymer micelles for drug delivery: design, characterization and biological significance. *Adv. Drug Deliv. Rev.* **47,** 113–131 (2001).
6. Nishiyama, N. & Kataoka, K. Current state, achievements, and future prospects of polymeric micelles as nanocarriers for drug and gene delivery. *Pharmacol Ther.* **112,** 630–648 (2006).
7. Matsumura, Y. & Maeda, H. A new concept for macromolecular therapeutics in cancer chemotherapy: mechanism of tumouritropic accumulation of proteins and the antitumour agent SMANCS. *Cancer Res.* **46,** 6387–6392 (1986).
8. Nishiyama, N. *et al.* Novel cisplatin-incorporated polymeric micelles can eradicate solid tumours in mice. *Cancer Res.* **63,** 8977–8983 (2003).
9. Bae, Y. *et al.* Preparation and biological characterization of polymeric micelle drug carriers with intracellular pH-triggered drug release property: tumor permeability, controlled subcellular drug distribution, and enhanced *in vivo* antitumor efficacy. *Bioconjug. Chem.* **16,** 122–130 (2005).
10. Cabral, H., Nishiyama, N. & Kataoka, K. Optimization of (1,2-diamino-cyclohexane) platinum(II)-loaded polymeric micelles directed to improved tumour targeting and enhanced antitumour activity. *J. Control. Release* **121,** 146–155 (2007).
11. Maruyama, K., Ishida, O., Takizawa, T. & Moribe, K. Possibility of active targeting to tumor tissue with liposome. *Adv. Drug Deliv. Rev.* **40,** 89–102 (1999).
12. Lammers, T. *et al.* Image-guided and passively tumor-targeted polymeric nanomedicines for radiochemotherapy. *Br. J. Cancer* **99,** 900–910 (2008).
13. Matsumura, Y. & Kataoka, K. Preclinical and clinical studies of anticancer agent-incorporating polymer micelles. *Cancer Sci.* **100,** 572–579 (2009).
14. Matsumura, Y. Preclinical and clinical studies of NK012, an SN-38-incorporating polymeric micelles, which is designed based on EPR effect. *Adv. Drug Deliv. Rev.* **63,** 184–192 (2011).

15. Working, P. K. *et al.* Pharmacokinetics, biodistribution and therapeutic efficacy of doxorubicin encapsulated in stealth liposomes (DOXIL). *J. Liposome Res.* **4,** 667–687 (1994).
16. Northfelt, D. W. *et al.* Pegylated-liposomal doxorubicin versus doxorubicin, bleomycin, and vincristine in the treatment of AIDS-related Kaposi's sarcoma: results of a randomized phase III clinical trial. *J. Clin. Oncol.* **16,** 2445–2451 (1998).
17. Gradishar, W. J. *et al.* Phase III trial of nanoparticle albumin-bound paclitaxel compared with polyethylated castor oil-based paclitaxel in women with breast cancer. *J. Clin. Oncol.* **23,** 7794–7803 (2005).
18. Uster, P. S., Working, P. K. & Vaage, J. Pegylated liposomal doxorubicin (DOXIL(R), CAELYX(R)) distribution in tumour models observed with confocal laser scanning microscopy. *Int. J. Pharm.* **162,** 77–86 (1998).
19. Unezaki, S. *et al.* Direct measurement of the extravasation of polyethyleneglycol-coated liposomes into solid tumor tissue by *in vivo* fluorescence microscopy. *Int. J. Pharm.* **144,** 11–17 (1996).
20. Kano, M. R. *et al.* Improvement of cancer-targeting therapy, using nanocarriers for intractable solid tumours by inhibition of TGF-β signaling. *Proc. Natl Acad. Sci. USA* **104,** 3460–3465 (2007).
21. Dreher, M. *et al.* Tumour vascular permeability, accumulation, and penetration of macromolecular drug carriers. *J. Natl Cancer Inst.* **98,** 330–343 (2006).
22. Perrault, S. D., Walkey, C., Jennings, T., Fischer, H. C. & Chan, W. C. W. Mediating tumour targeting efficiency of nanoparticles through design. *Nano Lett.* **9,** 1909–1915 (2009).
23. Aliabadi, H. M. & Lavasanifar, A. Polymeric micelles for drug delivery. *Exp. Opin. Drug. Deliv.* **3,** 139–162 (2006).
24. Matsumura, Y. *et al.* Phase I clinical trial and pharmacokinetic evaluation of NK911, a micelle-encapsulated doxorubicin. *Br. J. Cancer* **91,** 1775–1781 (2004).
25. Plummer, R. *et al.* A phase I clinical study of cisplatin-incorporated polymeric micelles (NC-6004) in patients with solid tumours. *Br. J. Cancer* **104,** 593–598 (2011).
26. Cabral, H., Nishiyama, N., Okazaki, S., Kato, Y. & Kataoka, K. Preparation and biological properties of dichloro(1,2-diaminocyclohexane)platinum(II) (DACHPt)-loaded polymeric micelles. *J. Control. Release* **101,** 223–232 (2005).
27. Nishiyama, N. & Kataoka, K. Preparation and characterization of size-controlled polymeric micelle containing *cis*-dichlorodiammineplatinum(II) in the core. *J. Control. Release* **74,** 83–94 (2001).
28. Murakami, M. *et al.* Improving drug potency and efficacy by nanocarrier-mediated subcellular targeting. *Sci. Transl. Med.* **3,** 64ra2 (2011).
29. Alexis, F., Pridgen, E., Molnar, L. K. & Farokhzad, O. C. Factors affecting the clearance and biodistribution of polymeric nanoparticles. *Mol. Pharm.* **5,** 505–515 (2008).
30. Verma, A. *et al.* Surface-structure-regulated cell-membrane penetration by monolayer-protected nanoparticles. *Nature Mater.* **7,** 588–595 (2008).
31. Kano, M. R. *et al.* Comparison of the effects of the kinase inhibitors imatinib, sorafenib, and transforming growth factor-β receptor inhibitor on extravasation of nanoparticles from neovasculature. *Cancer Sci.* **100,** 173–180 (2009).
32. Takahashi, Y. *et al.* Significance of vessel count, vascular endothelial growth factor, and its receptor (KDR) in intestinal-type gastric cancer. *Clin. Cancer Res.* **2,** 1679–1684 (1996).
33. Sofuni, A. *et al.* Differential diagnosis of pancreatic tumours using ultrasound contrast imaging. *J. Gastroenterol.* **40,** 518–525 (2005).
34. Matsumoto, Y. *et al.* Direct and instantaneous observation of intravenously injected substances using intravital confocal micro-videography. *Biomed. Optics Exp.* **1,** 1209–1216 (2010).
35. Choi, H. S. *et al.* Renal clearance of quantum dots. *Nature Biotechnol.* **25,** 1165–1170 (2007).
36. Terada, Y. *et al.* Construction and commissioning of BL37XU at SPring-8. *AIP Conf. Proc.* **705,** 376–379 (2004).

Acknowledgements

The authors are grateful to S. Fukuda from the University of Tokyo Hospital for his valuable support in conducting transmission electron microscopy and to S. Ogura for assistance with animal care. This study was supported by the Funding Program for World-Leading Innovative R&D on Science and Technology (FIRST Program) from the Japan Society for the Promotion of Science (JSPS) and Grants-in-Aid for Scientific Research from the Japanese Ministry of Health, Labour, and Welfare. μ-SR-XRF studies were supported by the Nanotechnology Support Program of the Japan Synchrotron Radiation Research Institute (JASRI).

Author contributions

H.C. designed and performed all the experiments. Y.M. assisted with *in vivo* confocal microscopies. K.M. and Y.T. helped in the μ-X-ray fluorescence measurements. Q.C. performed transmission electron microscopy of the micelles. M.M and M.K. aided in the biodistribution experiments. H.C. wrote the manuscript. M.R.K., K.M. and M.U. commented on the manuscript. N.N. and K.K. edited the manuscript. K.K., with help from N.N., supervised the whole project.

Additional information

The authors declare no competing financial interests. Supplementary information accompanies this paper at www.nature.com/naturenanotechnology. Reprints and permission information is available online at http://www.nature.com/reprints. Correspondence and requests for materials should be addressed to N.N. and K.K.

Journal of Controlled Release 149 (2011) 36–41

Contents lists available at ScienceDirect

Journal of Controlled Release

journal homepage: www.elsevier.com/locate/jconrel

Review

Progress in the development of ultrasound-mediated gene delivery systems utilizing nano- and microbubbles

Ryo Suzuki, Yusuke Oda, Naoki Utoguchi, Kazuo Maruyama *

Department of Biopharmaceutics, School of Pharmaceutical Sciences, Teikyo University, 1091-1 Suwarashi, Midori-ku, Sagamihara, Kanagawa 252-5195, Japan

ARTICLE INFO

Article history:
Received 28 December 2009
Accepted 6 May 2010
Available online 12 May 2010

Keywords:
Ultrasound
Microbubbles
Sonoporation
Gene delivery
Cavitation

ABSTRACT

Recently, ultrasound-mediated gene delivery with nano- and microbubbles was developed as a novel non-viral vector system. In this gene delivery system, microstreams and microjets, which are induced by disruption of nano/microbubbles exposed to ultrasound, are used as the driving force to transfer genes into cells by opening transient pores in the cell membrane. This system can directly deliver plasmid DNA and siRNA into cytosol without endocytosis pathway. Therefore, these genes are able to escape from degradation in lysosome and result in enhancing the efficiency of gene expression. In addition, it is expected that ultrasound-mediated gene delivery using nano/microbubbles would be a system to establish non-invasive and tissue specific gene expression because ultrasound can transdermally expose to target tissues and organs. This review focuses on the current ultrasound-mediated gene delivery system using nano/microbubbles. We discuss about the feasibility of this gene delivery system as novel non-viral vector system.

Contents

1. Introduction

Gene therapy has a potential in the treatment of cancer and diseases that are due to genomic causes. Viral vectors are efficient carriers of genes for transduction, but some problems have become evident [1–3]. Delivery vectors that are highly potent in terms of gene transduction efficiency should also be safe and easy to apply. Non-viral vectors have recently received focus as gene carriers, but their transduction efficiency is very low. Efforts have recently been directed towards improving this aspect [4–6]. Towards this end, ultrasound has been investigated for improving the efficiency of transgene delivery, and holds promise as a non-invasive gene delivery system.

Ultrasound shows potential for improving the efficiency of gene delivery into tissues and cells, a technique known as sonophoresis/sonoporation [7]. It is believed that ultrasound perturbs cell membranes and causes transient pores to open in the membrane, thus facilitating gene entry into the cell [8]. In addition, it has been reported that microbubbles utilized as ultrasound contrast agents play an important role in enhancing the efficiency of gene delivery, without causing cell damage [9]. In general, cell damage is dependent on ultrasound intensity, concentration of microbubbles and cell type. Especially, ultrasound intensity and exposure time are key factors. Therefore, it is important to optimize the condition of ultrasound exposure in ultrasound-mediated gene delivery [10–13]. Some researchers studied about the cell damage by the disruption of microbubbles with ultrasound exposure [14–19]. These reports are useful as informative references for ultrasound-mediated gene delivery utilizing microbubbles.

* Corresponding author. Tel.: +81 42 685 3722; fax: +81 42 685 3432.
E-mail address: maruyama@pharm.teikyo-u.ac.jp (K. Maruyama).

0168-3659/$ – see front matter © 2010 Elsevier B.V. All rights reserved.
doi:10.1016/j.jconrel.2010.05.009

Microbubbles which are destroyed by ultrasound exposure generate microstreams or microjets, resulting in shear stress to cells and the generation of transient holes in cell membranes [20]. Since this approach can be used to deliver extracellular molecules such as genes into cells, microbubbles could facilitate ultrasound-mediated gene delivery. In addition, submicron sized bubbles (nanobubbles), which are smaller than conventional microbubbles, were recently reported [21,22], and we have also developed novel liposomal nanobubbles (Bubble liposomes) [11,23–32]. These nanobubbles can also be utilized as enhancing tool of gene delivery efficiency in ultrasound-mediated gene delivery. In this review, we introduced about ultrasound-mediated delivery systems combined with nano/microbubbles and discussed the feasibility as non-viral vector system.

2. Microbubbles as ultrasound contrast agents

Ultrasonography is a widely used diagnostic medical imaging technique that is non-invasive, relatively low-cost, easy to use, provides real-time imaging, and importantly, avoids the use of hazardous ionizing radiation. Ultrasound wave pulses generated by an ultrasound transducer are partially reflected or scattered by the interfaces between different tissues. The transducer detects the ultrasound waves returned by scattering, and these signals are converted to ultrasound images. Since blood scatters ultrasound poorly, ultrasound contrast agents, which increase the scattering and reflection of ultrasound waves, are utilized for blood flow imaging, especially in cardiosonography. Gramiak and Shah in 1968 were the first to use contrast agents in echocardiography [33], and reported that the aortic delineation was improved by intracardiac injection of agitated saline containing air bubbles. However, these air microspheres disappeared within a few seconds following intravenous injection due to the high solubility of air in blood, and the impossibility of larger air bubbles to pass through pulmonary capillaries. For these reasons, it is difficult to use injected conventional air bubbles for opacifying the left cardiac chambers, unless they are injected by the intracoronary or aortic route.

To improve the stability and decrease the size of air bubbles, microbubbles with a thin shell such as albumin (Albunex) or galactose palmitic acid (Levovist) have been developed (Table 1). These bubbles are first-generation microbubbles, and are air-filled microspheres. Their mean diameter ranges from 1 to 8 μm, and they are capable of passing through pulmonary capillaries. However, these air-filled microbubbles disappear from the bloodstream within seconds after administration because of their low resistance to arterial pressure gradients, and the high solubility of air in blood [34]. Approaches for increasing the stability of microbubbles and decreasing the solubility of their gas in blood are clearly required, and lead to the development of microbubbles filled with a high molecular weight hydrophobic gas such as perfluorocarbons or sulfur hexafluoride. These microbubbles represent second-generation contrast agents, in which surfactants, sonicated albumin and phospholipids are used to form the bubble shell in order to improve microbubble stability in the bloodstream. The acoustic backscatter of these microbubbles is higher than that of blood and organs, due to differences in acoustic impedance between gases, and blood or organs. Therefore, microbubbles are useful contrast agents, especially in echocardiography. In addition, Sonazoid which was a phosphatidylserine-stabilized perfluorobutane microbubbles was developed as a useful contrast agent for hepatic tumors [35–37]. This is due to uniqueness of Sonazoid whose microbubbles are likely to be taken up by Kupffer cells (liver macrophages) in the healthy liver and enhances contrast of the liver parenchyma during the delayed phase, which usually occurs within 10 min after the injection. In contrast, tumor that lacks Kupffer cells was not enhanced resulting in clear negative contrast of the tumor [36]. Thus, Sonazoid is a new type of microbubble which is able to target Kupffer cells. However, Sonazoid has been commercially available microbubble for clinical use only in Japan since 2007. In the future, it is expected that tissue specific targeting bubbles such as Sonazoid are developed.

Table 1
Ultrasound contrast agents.

Name	Shell	Entrapping gas	Size (μm)
Albunex	Albumin	Air	4.3
Levovist	Galactose	Air	2–4
Optison	Albumin	Perfluoropropane	3–32
Definity	Lipids	Perfluoropropane	1.1–20
Imagent	Lipids	Perfluoropropane	5
Sonovue	Lipids	Sulphur hexafluoride	2.5
Sonazoid	Lipids	Perfluorobutane	2–3

3. Properties of microbubbles combined with ultrasound

The behavior of microbubbles depends on the amplitude of ultrasound used. At very low acoustic pressure (mechanical index (MI)<0.05–0.1), the microbubbles cause linear oscillation, and the reflected frequency is equal to the transmitted frequency (Fig. 1(a)). An increase in acoustic pressure (0.1<MI<0.3), referred to as low-power imaging, causes non-linear expansion and compression of the microbubbles (Fig. 1(b)). In fact, the bubble becomes somewhat more resistant to compression than to expansion. This phenomenon is known as stable or non-inertial cavitation, and results in the emission of non-linear harmonic signals at multiples of the transmitted frequency [38]. Harmonic imaging with microbubbles enhances the bubbles-to-tissue backscatter signal ratio, due to insignificant harmonic backscatter from tissue in this range of MI. Therefore, this technique can improve the signal-noise ratio and be useful in left ventricular pacification imaging [39]. In addition, stable or non-inertial cavitation can enhance transient cell membrane permeability (Fig. 2(a)) [40]. Machluf et al. reported that ultrasound exposure (0.16 MI, 1 MHz) in the presence of microbubbles deliver plasmid DNA into cells [41,42].

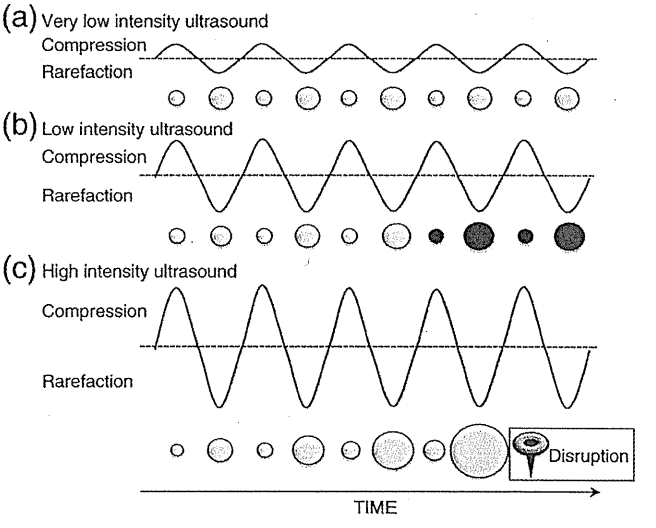

Fig. 1. Scheme showing microbubble behavior in acoustic fields (a) Very low intensity ultrasound induces linear oscillation of the microbubble. (b) Low intensity ultrasound induces oscillation of the microbubble with a gradual increase in microbubble diameter until it reaches a resonant diameter, at which point stable oscillation occurs (filled black circles). (c) High intensity ultrasound causes a rapid increase in the diameter of the microbubble for a few cycles, which induces bubble disruption.

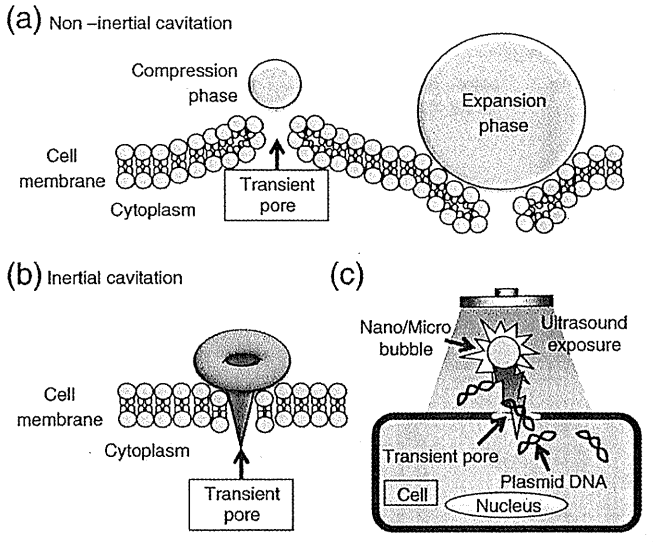

Fig. 2. Scheme showing the pore formation in the cell membrane by oscillating or disrupting microbubble (a) The pushing and pulling behavior (non-inertial cavitation) of the microbubble and (b) the collapse of microbubbles (inertial cavitation) cause rupture of the cell membrane creating pore allowing trans-membrane flux of fluid and macromolecules such as plasmid DNA and oligonucleotides (c).

Higher acoustic pressure (MI>0.3–0.6) causes forced expansion and compression of microbubbles and results in bubble disruption (collapse) (Fig. 1(c)). This inertial cavitation involved in bubble disruption is utilized as flash-replenishment in reperfusion study of diagnosis [43]. This inertial cavitation induces microstreams/microjets around the bubbles. The peak velocity of the microstreams/microjets can reach 700 m/s. These microstreams/microjets can enhance the permeability of cell membranes due to the formation of transient pores (Fig. 2(b)) [20]. In the presence of nano-/microbubbles, the threshold for cavitation decreases, and it results in rendering their destruction feasible at lower energies of ultrasound.

4. Gene delivery using sonoporation as a non-viral vector system

The first studies investigating the utility of ultrasound for gene delivery used frequencies in the range 20–50 kHz [7,44]. However, these frequencies, along with cavitation, are known to cause tissue damage if not properly controlled [45,46]. To overcome this problem, many gene delivery studies have used therapeutic ultrasound, which operates at frequencies of 1–3 MHz, intensities of 0.5–2.5 W/cm^2 or MI 0.3–2, and in pulse-mode [47]. However, as these conditions result in very inefficient gene delivery, therapeutic ultrasound combined with nano/microbubble contrast agents has been investigated for enhancing gene transfection efficiency [9,13,48,49]. This combination method has many of the characteristics required for practical gene therapy including low toxicity, the potential for repeated applications, organ specificity and broad applicability to acoustically accessible organs. Under proper conditions, the combination of ultrasound and nano/microbubbles can create transient non-lethal perforations in cell membranes. Taniyama et al. reported that transient pores formed in cell membranes upon exposure to ultrasound and Optison, and that the pores completely closed [20]. In addition, the behavior of insonated microbubbles was observed with high-speed camera microscopy [50]. Exposure to high intensity ultrasound induced complete disruption of the microbubbles. The above findings suggest that the combination of microbubbles and ultrasound could be useful for gene delivery (Fig. 2(c)).

4.1. Applying to plasmid DNA delivery

Much research has been conducted both *in vitro* and *in vivo* into gene delivery using ultrasound to disrupt microbubbles. In early feasibility studies, reporter genes such as luciferase, β-galactosidase and green fluorescent protein (GFP) were utilized to assess transfection efficiency [13,51–54]. Transfection method in *in vitro* study is very simple. In general, cells suspended with microbubbles and plasmid DNA were exposed with ultrasound for a few second-several tens of seconds due to be completed transfection in a short period of time [27]. Transfection efficiency is affected by ultrasound exposure condition such as intensity, frequency, period, duty cycle, or type and concentration of microbubble [10,11,13,14]. Normally, the efficiency increase according to increasing ultrasound intensity and period [11]. On the other hand, it was reported that the efficiency and cell viability by the transfection with fractionated exposure was higher than that with continuous exposure in the same period of total exposure [19]. In addition, it was reported that there was optimal concentration of microbubbles [55]. Unfortunately, optimal condition is not completely clear in the transfection using this system because of many changeable parameters as mentioned above. Thus, some researchers have studies the properties of this transfection technology to find out optimal condition.

Many of *in vivo* early studies focused on organs and tissues that are readily imaged by diagnostic ultrasonography, including heart [52,56], skeletal muscle [51] and kidney [57]. Bekeredjian et al. reported the use of ultrasound and microbubbles to deliver reporter genes into heart [56]. Subsequently, Korpanty et al. succeeded in delivering the gene for vascular endothelial growth factor (VEGF) into heart using the same gene delivery system, and VEGF-mediated angiogenesis to rat myocardium [58]. This technique has begun to be broadly utilized as a gene delivery system to other organs, tissues and cells such as the vascular system, pancreas, central nerve system, tumors, and hematopoietic cells. For example, Shimamura et al. reported transfection to the central nervous system by sonoporation after injection of a reporter gene and Optison into cistern magna or striatum [59]. In this study, transfection by microbubbles using ultrasound transferred the reporter gene into cells around the neurons, and not into the neuron cells themselves. Takahashi et al. reported gene transfer into the spine using ultrasound and microbubbles [60]. In addition, Aoi et al. developed herpes simplex virus mediated thymidine kinase (HSV-tk)-mediated suicide gene therapy using nanobubbles and ultrasound [61]. In this therapy, HSV-tk corded plasmid DNA and nanobubbles were injected into tumor tissue of mice, and ultrasound was transdermally exposed toward the tissue. The reduction of tumor size was observed by administration of ganciclovir in the mice transfected HSV-tk corded plasmid DNA with nanobubbles and ultrasound. Previously, we developed novel liposomal nanobubble (Bubble liposome) entrapping perfluoropropane gas (Fig. 3(a–c)) [11,27]. The size of Bubble liposomes was about 500 nm and they were much smaller than Sonazoid (Fig. 3(b)). Bubble liposome could also utilize as an effective plasmid DNA delivery tool *in vitro* (Fig. 3(d)) and *in vivo* by the combination with ultrasound. We reported the utility of Bubble liposome in cancer gene therapy using interleukin-12 (IL-12) corded plasmid DNA [24]. The combination of Bubble liposomes and ultrasound dramatically suppressed tumor growth (Fig. 4). As mentioned above, sonoporation combined with nano/microbubbles could be a good system for plasmid DNA delivery.

4.2. Applying to oligonucleotide delivery

Oligonucleotides such as antisense, decoy and small interfering RNA (siRNA) are important molecules that can stop the expression of specific genes [62,63]. In particular, RNA interference (RNAi) using siRNA has potential in the development of new treatments for disease,

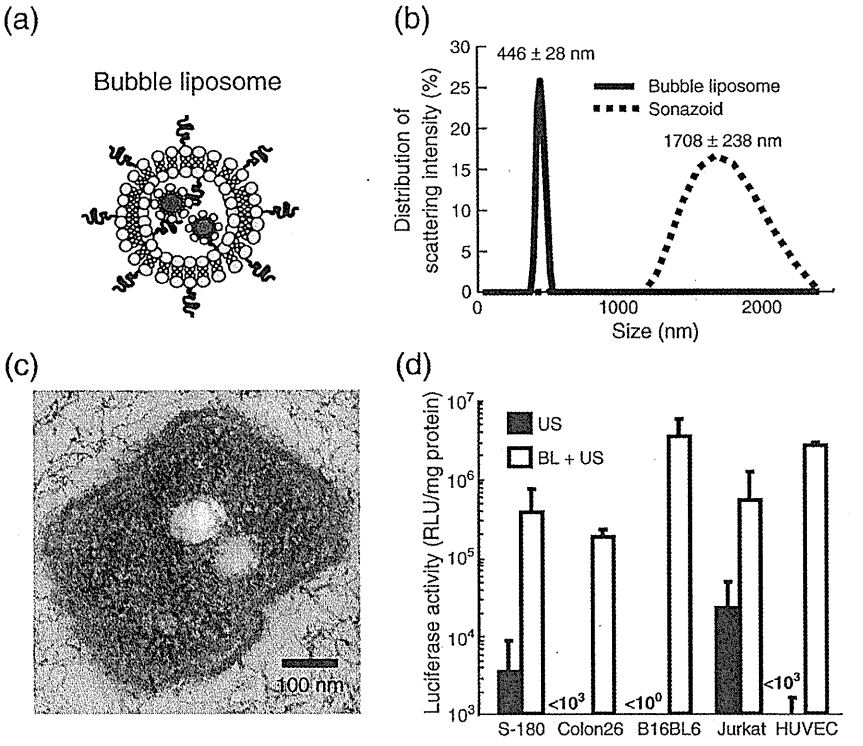

Fig. 3. Comparison of microbubbles and Bubble liposomes (a) Schematic of Bubble liposome. (b) Size distribution of Sonazoid and Bubble liposomes as measured by dynamic light scattering. (c) Transmission electron microscopy (50,000×) of Bubble liposome. (d) Luciferase expression in various types of cells transfected using Bubble liposomes and ultrasound. Cells (1×10^5 cells/500 μL) mixed with pCMV-Luc (5 μg) and Bubble liposomes (60 μg) were exposed or not to ultrasound (frequency, 2 MHz; duty, 50%; burst rate, 2 Hz; intensity, 2.5 W/cm^2; time 10 s). The cells were washed and cultured for 2 days. Thereafter, luciferase activity was determined with luminometer. Data are shown as means ± S.D. ($n=3$). BL, Bubble liposome, pCMV-Luc: luciferase corded plasmid DNA, HUVEC: human umbilical vascular endothelial cell.

including malignant, infectious and autoimmune diseases. In order to achieve efficient gene silencing, it is important that the siRNA is introduced into the cytoplasm of the target cell [64]. Diverse approaches have been attempted to develop efficient oligonucleotide delivery methods [62]. However, technologies that enable the tissue-targeted delivery of siRNA using non-viral vectors need improvement.

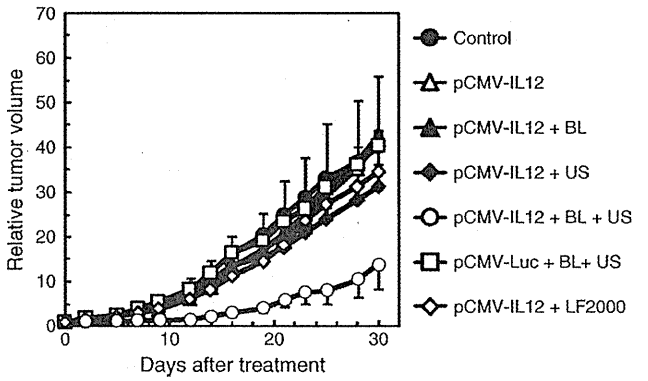

Fig. 4. Cancer gene therapy by IL-12 gene delivery with Bubble liposomes and ultrasound B6C3F1 mice were intradermally inoculated with 1×10^6 OV-HM cells into the flank. On day 7 after tumor inoculation, the tumors were injected with pCMV-IL12 (10 μg) using Bubble liposomes (2.5 μg) and/or ultrasound (1 MHz, 0.7 W/cm^2, 1 min), or Lipofectamine 2000 as a conventional lipofection method. (b) Therapeutic effect was assessed by measuring tumor growth. The volume of the growing tumors was calculated by: (tumor volume; mm^3) = (major axis; mm) × (minor axis; mm)^2 × 0.5). The data are represented as tumor volume relative to the tumor volume on day 7 after tumor inoculation. Each point represents the mean ± SD ($n=5$). BL: Bubble liposomes, US: Ultrasound, LF2000: Lipofectamine 2000, pCMV-IL-12: IL-12 corded plasmid DNA, pCMV-Luc: Luciferase corded plasmid DNA.

As mentioned above, the combination of ultrasound and nano/microbubbles can directly deliver extracellular molecules into the cytosol [25], where antisense, decoy and siRNA function, so this delivery system might better exhibit the functions of these oligonucleotides. Azuma et al. reported that NF-κB decoy delivery into transplanted kidney by the combination of microbubbles and ultrasound could significantly decrease IL-1β and TNF-α (inflammatory cytokines) and prolonged the survival rate of kidney-transplanted mice [57]. Negishi et al. reported that siRNA was directly introduced into the cytoplasm by nanobubbles and ultrasound [30]. In addition, transfection of siRNA into tibialis muscles with nanobubble and ultrasound resulted in gene-silencing, which was sustained for more than 3 weeks. It therefore appears that the combination of nano/microbubbles and ultrasound could be a useful siRNA delivery system. In addition, siRNA transfection with ultrasound and microbubbles was utilized to apply to mesenchymal stem cells, indicating that this technique could be applicable to genetically modified stem cell therapy. Vandenbroucke et al. also developed an interesting siRNA delivery system using sonoporation [65]. They coupled (PEG-siPlex) of PEGylated cationic liposomes and siRNA, and introduced the complex into gas-filled lipid microbubbles. Both the microbubbles and PEG-siPlex, which were modified with biotin, were attached via avidin. Although PEG-siPlex can protect siRNA from digestion by nucleases *in vivo*, PEGylation makes it difficult for the siRNA to be recognized and taken up by the target cells. The microbubble/sonication system should be able to overcome the negative effects of PEGylating siRNA-cationic liposomes (siPlex) and enhance the efficiency of ultrasound-assisted siRNA delivery. Although siRNA delivery mediated by ultrasound and nano/microbubbles must be optimized, this system may open up new perspectives for ultrasound-controlled *in vivo* siRNA delivery.

5. Efforts to tissue- or organ-selective gene delivery

To establish ideal gene therapy, it is important to deliver therapeutic gene into target tissue or organ. In the early study, gene and nano/microbubbles were directly injected into target tissue and organ [53,66]. However, in this method, there are some limitations such as injection volume and injection technique. To improve these problems, some researchers recently developed ultrasound-mediated gene delivery by the supplying gene and nano/microbubbles via blood flow [11,67]. In this delivery, gene expression was limited in the area exposed ultrasound. Ultrasound can be easily focused to a target tissue or organ. Therefore, it might be possible to develop an optimal tissue- or organ-specific gene delivery system by combining nano/microbubble targeting and focused ultrasound. Shen et al. succeeded to developed ultrasound-mediated gene expression in liver via intraportal injection of plasmid DNA and microbubbles [68]. Grayburn et al. reported insulin expression following insulin gene delivery to pancreatic islets in rat by a combination of microbubbles and ultrasound exposure and succeeded to decrease blood glucose level in diabetes rat [67,69]. We also developed the gene delivery into tumor tissue by the combination of injection from tumor dominant artery and ultrasound exposure toward tumor tissue [11]. In addition, transdermal ultrasound exposure toward liver could induce liver selective gene expression after systemic injection of plasmid DNA and Bubble liposomes. In this case, luciferase expression was dominantly observed in the parenchymal cells of liver. These results suggested that Bubble liposomes could quickly transduce plasmid DNA into each tissue by cavitation even under the existence of blood stream. Moreover, we developed the combination method using mannosylated lipoplexes and Bubble liposomes with ultrasound to enhance gene transfection in mannose receptor-expressing cells in liver [29]. In this study, after systemic injection of mannosylated lipoplex, Bubble liposomes were systemically injected and ultrasound was transdermally exposed toward liver. Gene expression was observed mannose receptor-expressing cells such as macrophage and dendritic cells which were known as antigen presenting cells. It is expected that ultrasound-mediated gene delivery with nano/microbubbles might be useful to develop target tissue or organ-selective gene delivery in vivo.

Previously, several groups have reported active targetable nano/microbubbles to endothelium [70], rejected tissues [71], neovasculature endothelium [72], lymph node-related vasculature [73] and activated platelets[74] by targeting ICAM-1 [75], VCAM-1 [76] or integrins [77]. We also developed blood clot targetable Bubble liposomes modified with arginine-glycine-aspartic acid (RGD) peptides to develop effective ultrasound contrast agents for blood clots imaging [78]. Although these nano/microbubbles were developed as ultrasound imaging agents, it might be possible to develop an optimal tissue- or organ-selective gene delivery system by combining targetable nano/microbubble associated with gene and ultrasound.

6. Conclusion

Ultrasound has long been utilized as a useful diagnostic tool. Therapeutic ultrasound was recently developed and is being utilized in clinical settings. The combination of therapeutic ultrasound and nano/microbubbles is an interesting and important system for establishing a novel and non-invasive gene delivery system. Gene expression efficiency with this system can effectively deliver gene compared with conventional non-viral vector system such as lipofection method due to deliver gene into cytosol without endocytosis pathway. Many *in vivo* studies has been reported about ultrasound-mediated gene delivery with nano/microbubbles. Especially, there are some reports about feasibility studies of gene therapy for various diseases [24,29,61,67] In addition, this system has a potency of site specific gene delivery by the control of ultrasound exposure site. Therefore, it is expected that this technology would be utilized as a novel gene delivery system in clinical field.

References

[1] E. Check, Safety panel backs principle of gene-therapy trials, Nature 420 (2002) 595.
[2] E. Check, Second cancer case halts gene-therapy trials, Nature 421 (2003) 305.
[3] E. Marshall, Gene therapy death prompts review of adenovirus vector Science 286 (1999) 2244–2245.
[4] K. Kogure, H. Akita, Y. Yamada, H. Harashima, Multifunctional envelope-type nano device (MEND) as a non-viral gene delivery system, Adv. Drug Deliv. Rev. 60 (2008) 559–571.
[5] F. Liu, C.C. Conwell, X. Yuan, L.M. Shollenberger, L. Huang, Novel nonviral vectors target cellular signaling pathways: regulated gene expression and reduced toxicity, J. Pharmacol. Exp. Ther. 321 (2007) 777–783.
[6] K. Itaka, S. Ohba, K. Miyata, H. Kawaguchi, K. Nakamura, T. Takato, U.I. Chung, K. Kataoka, Bone regeneration by regulated in vivo gene transfer using biocompatible polyplex nanomicelles, Mol. Ther. 15 (2007) 1655–1662.
[7] M. Fechheimer, J.F. Boylan, S. Parker, J.E. Sisken, G.L. Patel, S.G. Zimmer, Transfection of mammalian cells with plasmid DNA by scrape loading and sonication loading, Proc. Natl. Acad. Sci. U. S. A. 84 (1987) 8463–8467.
[8] M.W. Miller, D.L. Miller, A.A. Brayman, A review of in vitro bioeffects of inertial ultrasonic cavitation from a mechanistic perspective, Ultrasound Med. Biol. 22 (1996) 1131–1154.
[9] W.J. Greenleaf, M.E. Bolander, G. Sarkar, M.B. Goldring, J.F. Greenleaf, Artificial cavitation nuclei significantly enhance acoustically induced cell transfection, Ultrasound Med. Biol. 24 (1998) 587–595.
[10] L.B. Feril Jr., R. Ogawa, K. Tachibana, T. Kondo, Optimized ultrasound-mediated gene transfection in cancer cells, Cancer Sci. 97 (2006) 1111–1114.
[11] R. Suzuki, T. Takizawa, Y. Negishi, N. Utoguchi, K. Sawamura, K. Tanaka, E. Namai, Y. Oda, Y. Matsumura, K. Maruyama, Tumor specific ultrasound enhanced gene transfer in vivo with novel liposomal bubbles, J. Control. Release 125 (2008) 137–144.
[12] S.V. Pislaru, C. Pislaru, R.R. Kinnick, R. Singh, R. Gulati, J.F. Greenleaf, R.D. Simari, Optimization of ultrasound-mediated gene transfer: comparison of contrast agents and ultrasound modalities, Eur. Heart J. 24 (2003) 1690–1698.
[13] T. Li, K. Tachibana, M. Kuroki, M. Kuroki, Gene transfer with echo-enhanced contrast agents: comparison between Albunex, Optison, and Levovist in mice–initial results, Radiology 229 (2003) 423–428.
[14] M.A. Hassan, M.A. Buldakov, R. Ogawa, Q.L. Zhao, Y. Furusawa, N. Kudo, T. Kondo, P. Riesz, Modulation control over ultrasound-mediated gene delivery: evaluating the importance of standing waves, J. Control. Release 141 (2010) 70–76.
[15] D.J. Wells, Electroporation and ultrasound enhanced non-viral gene delivery in vitro and in vivo, Cell Biol. Toxicol. 26 (2010) 21–28.
[16] M.A. Hassan, L.B. Feril Jr., K. Suzuki, N. Kudo, K. Tachibana, T. Kondo, Evaluation and comparison of three novel microbubbles: enhancement of ultrasound-induced cell death and free radicals production, Ultrason. Sonochem. 16 (2009) 372–378.
[17] L.B. Feril Jr., T. Kondo, Q.L. Zhao, R. Ogawa, K. Tachibana, N. Kudo, S. Fujimoto, S. Nakamura, Enhancement of ultrasound-induced apoptosis and cell lysis by echo-contrast agents, Ultrasound Med. Biol. 29 (2003) 331–337.
[18] N. Kudo, K. Okada, K. Yamamoto, Sonoporation by single-shot pulsed ultrasound with microbubbles adjacent to cells, Biophys. J. 96 (2009) 4866–4876.
[19] D.P. Guo, X.Y. Li, P. Sun, Y.B. Tang, X.Y. Chen, Q. Chen, L.M. Fan, B. Zang, L.Z. Shao, X.R. Li, Ultrasound-targeted microbubble destruction improves the low density lipoprotein receptor gene expression in HepG2 cells, Biochem. Biophys. Res. Commun. 343 (2006) 470–474.
[20] Y. Taniyama, K. Tachibana, K. Hiraoka, T. Namba, K. Yamasaki, N. Hashiya, M. Aoki, T. Ogihara, K. Yasufumi, R. Morishita, Local delivery of plasmid DNA into rat carotid artery using ultrasound, Circulation 105 (2002) 1233–1239.
[21] Z. Gao, A.M. Kennedy, D.A. Christensen, N.Y. Rapoport, Drug-loaded nano/microbubbles for combining ultrasonography and targeted chemotherapy, Ultrasonics 48 (2008) 260–270.
[22] Y. Wang, X. Li, Y. Zhou, P. Huang, Y. Xu, Preparation of nanobubbles for ultrasound imaging and intracelluar drug delivery, Int. J. Pharm. 384 (2010) 148–153.
[23] R. Suzuki, K. Maruyama, Effective in vitro and in vivo gene delivery by the combination of liposomal bubbles (bubble liposomes) and ultrasound exposure, Methods Mol. Biol. 605 (2009) 473–486.
[24] R. Suzuki, E. Namai, Y. Oda, N. Nishiie, S. Otake, R. Koshima, K. Hirata, Y. Taira, N. Utoguchi, Y. Negishi, S. Nakagawa, K. Maruyama, Cancer gene therapy by IL-12 gene delivery using liposomal bubbles and tumoral ultrasound exposure, J. Control. Release 142 (2010) 245–250.
[25] R. Suzuki, Y. Oda, N. Utoguchi, E. Namai, Y. Taira, N. Okada, N. Kadowaki, T. Kodama, K. Tachibana, K. Maruyama, A novel strategy utilizing ultrasound for antigen delivery in dendritic cell-based cancer immunotherapy, J. Control. Release 133 (2009) 198–205.
[26] R. Suzuki, T. Takizawa, Y. Kuwata, M. Mutoh, N. Ishiguro, N. Utoguchi, A. Shinohara, M. Eriguchi, H. Yanagie, K. Maruyama, Effective anti-tumor activity of oxaliplatin encapsulated in transferrin-PEG-liposome, Int. J. Pharm. 346 (2008) 143–150.
[27] R. Suzuki, T. Takizawa, Y. Negishi, K. Hagisawa, K. Tanaka, K. Sawamura, N. Utoguchi, T. Nishioka, K. Maruyama, Gene delivery by combination of novel liposomal bubbles with perfluoropropane and ultrasound, J. Control. Release 117 (2007) 130–136.
[28] R. Suzuki, T. Takizawa, Y. Negishi, N. Utoguchi, K. Maruyama, Effective gene delivery with liposomal bubbles and ultrasound as novel non-viral system, J. Drug Target. 15 (2007) 531–537.

[29] K. Un, S. Kawakami, R. Suzuki, K. Maruyama, F. Yamashita, M. Hashida, Enhanced transfection efficiency into macrophages and dendritic cells by a combination method using mannosylated lipoplexes and bubble liposomes with ultrasound exposure, Hum. Gene Ther. 21 (2010) 65–74.

[30] Y. Negishi, Y. Endo, T. Fukuyama, R. Suzuki, T. Takizawa, D. Omata, K. Maruyama, Y. Aramaki, Delivery of siRNA into the cytoplasm by liposomal bubbles and ultrasound, J. Control. Release 132 (2008) 124–130.

[31] Y. Negishi, D. Omata, H. Iijima, Y. Takabayashi, K. Suzuki, Y. Endo, R. Suzuki, K. Maruyama, M. Nomizu, Y. Aramaki, Enhanced laminin-derived peptide AG73-mediated liposomal gene transfer by bubble liposomes and ultrasound, Mol. Pharm. 7 (2010) 217–226.

[32] T. Yamashita, S. Sonoda, R. Suzuki, N. Arimura, K. Tachibana, K. Maruyama, T. Sakamoto, A novel bubble liposome and ultrasound-mediated gene transfer to ocular surface: RC-1 cells in vitro and conjunctiva in vivo, Exp. Eye Res . 85 (2007) 741–748.

[33] P.M. Shah, R. Gramiak, D.H. Kramer, P.N. Yu, Determinants of atrial (S4) and ventricular (S3) gallop sounds in primary myocardial disease, N Engl J. Med. 278 (1968) 753–758.

[34] A. Kabalnov, D. Klein, T. Pelura, E. Schutt, J. Weers, Dissolution of multicomponent microbubbles in the bloodstream: 1, Theory Ultrasound Med Biol 24 (1998) 739–749.

[35] K. Yanagisawa, F. Moriyasu, T. Miyahara, M. Yuki, H. Iijima, Phagocytosis of ultrasound contrast agent microbubbles by Kupffer cells, Ultrasound Med. Biol. 33 (2007) 318–325.

[36] R. Watanabe, M. Matsumura, T. Munemasa, M. Fujimaki, M. Suematsu, Mechanism of hepatic parenchyma-specific contrast of microbubble-based contrast agent for ultrasonography: microscopic studies in rat liver, Invest. Radiol. 42 (2007) 643–651.

[37] K. Korenaga, M. Korenaga, M. Furukawa, T. Yamasaki, I. Sakaida, Usefulness of Sonazoid contrast-enhanced ultrasonography for hepatocellular carcinoma: comparison with pathological diagnosis and superparamagnetic iron oxide magnetic resonance images, J. Gastroenterol. 44 (2009) 733–741.

[38] E.C. Unger, E. Hersh, M. Vannan, T.O. Matsunaga, T. McCreery, Local drug and gene delivery through microbubbles, Prog. Cardiovasc. Dis. 44 (2001) 45–54.

[39] S.L. Mulvagh, A.N. DeMaria, S.B. Feinstein, P.N. Burns, S. Kaul, J.G. Miller, M. Monaghan, T.R. Porter, L.J. Shaw, F.S. Villanueva, Contrast echocardiography: current and future applications, J. Am. Soc. Echocardiogr. 13 (2000) 331–342.

[40] A. van Wamel, K. Kooiman, M. Harteveld, M. Emmer, F.J. ten Cate, M. Versluis, N. de Jong, Vibrating microbubbles poking individual cells: drug transfer into cells via sonoporation, J. Control. Release 112 (2006) 149–155.

[41] M. Duvshani-Eshet, L. Baruch, E. Kesselman, E. Shimoni, M. Machluf, Therapeutic ultrasound-mediated DNA to cell and nucleus: bioeffects revealed by confocal and atomic force microscopy, Gene Ther. 13 (2006) 163–172.

[42] M. Duvshani-Eshet, D. Adam, M. Machluf, The effects of albumin-coated microbubbles in DNA delivery mediated by therapeutic ultrasound, J. Control. Release 112 (2006) 156–166.

[43] K. Kalantarinia, J.T. Belcik, J.T. Patrie, K. Wei, Real-time measurement of renal blood flow in healthy subjects using contrast-enhanced ultrasound, Am. J. Physiol. Ren. Physiol 297 (2009) F1129–F1134.

[44] M. Joersbo, J. Brunstedt, Protein synthesis stimulated in sonicated sugar beet cells and protoplasts, Ultrasound Med. Biol. 16 (1990) 719–724.

[45] H.R. Guzman, A.J. McNamara, D.X. Nguyen, M.R. Prausnitz, Bioeffects caused by changes in acoustic cavitation bubble density and cell concentration: a unified explanation based on cell-to-bubble ratio and blast radius, Ultrasound Med. Biol. 29 (2003) 1211–1222.

[46] W. Wei, B. Zheng-zhong, W. Yong-jie, Z. Qing-wu, M. Ya-lin, Bioeffects of low-frequency ultrasonic gene delivery and safety on cell membrane permeability control, J. Ultrasound Med. 23 (2004) 1569–1582.

[47] H.J. Kim, J.F. Greenleaf, R.R. Kinnick, J.T. Bronk, M.E. Bolander, Ultrasound-mediated transfection of mammalian cells, Hum. Gene Ther. 7 (1996) 1339–1346.

[48] D.M. Hallow, A.D. Mahajan, T.E. McCutchen, M.R. Prausnitz, Measurement and correlation of acoustic cavitation with cellular bioeffects, Ultrasound Med. Biol. 32 (2006) 1111–1122.

[49] R.V. Shohet, S. Chen, Y.T. Zhou, Z. Wang, R.S. Meidell, R.H. Unger, P.A. Grayburn, Echocardiographic destruction of albumin microbubbles directs gene delivery to the myocardium, Circulation 101 (2000) 2554–2556.

[50] A. van Wamel, A. Bouakaz, M. Versluis, N. de Jong, Micromanipulation of endothelial cells: ultrasound-microbubble-cell interaction, Ultrasound Med. Biol. 30 (2004) 1255–1258.

[51] J.P. Christiansen, B.A. French, A.L. Klibanov, S. Kaul, J.R. Lindner, Targeted tissue transfection with ultrasound destruction of plasmid-bearing cationic microbubbles, Ultrasound Med. Biol. 29 (2003) 1759–1767.

[52] S. Chen, R.V. Shohet, R. Bekeredjian, P. Frenkel, P.A. Grayburn, Optimization of ultrasound parameters for cardiac gene delivery of adenoviral or plasmid deoxyribonucleic acid by ultrasound-targeted microbubble destruction, J. Am. Coll. Cardiol. 42 (2003) 301–308.

[53] Q.L. Lu, H.D. Liang, T. Partridge, M.J. Blomley, Microbubble ultrasound improves the efficiency of gene transduction in skeletal muscle in vivo with reduced tissue damage, Gene Ther. 10 (2003) 396–405.

[54] S. Tsunoda, O. Mazda, Y. Oda, Y. Iida, S. Akabame, T. Kishida, M. Shin-Ya, H. Asada, S. Gojo, J. Imanishi, H. Matsubara, T. Yoshikawa, Sonoporation using microbubble BR14 promotes pDNA/siRNA transduction to murine heart, Biochem. Biophys. Res. Commun. 336 (2005) 118–127.

[55] Y. Taniyama, K. Tachibana, K. Hiraoka, M. Aoki, S. Yamamoto, K. Matsumoto, T. Nakamura, T. Ogihara, Y. Kaneda, R. Morishita, Development of safe and efficient novel nonviral gene transfer using ultrasound: enhancement of transfection efficiency of naked plasmid DNA in skeletal muscle, Gene Ther. 9 (2002) 372–380.

[56] R. Bekeredjian, S. Chen, P.A. Frenkel, P.A. Grayburn, R.V. Shohet, Ultrasound-targeted microbubble destruction can repeatedly direct highly specific plasmid expression to the heart, Circulation 108 (2003) 1022–1026.

[57] H. Azuma, N. Tomita, Y. Kaneda, H. Koike, T. Ogihara, Y. Katsuoka, R. Morishita, Transfection of NFkappaB-decoy oligodeoxynucleotides using efficient ultrasound-mediated gene transfer into donor kidneys prolonged survival of rat renal allografts, Gene Ther. 10 (2003) 415–425.

[58] G. Korpanty, S. Chen, R.V. Shohet, J. Ding, B. Yang, P.A. Frenkel, P.A. Grayburn, Targeting of VEGF-mediated angiogenesis to rat myocardium using ultrasonic destruction of microbubbles, Gene Ther. 12 (2005) 1305–1312.

[59] M. Shimamura, N. Sato, Y. Taniyama, S. Yamamoto, M. Endoh, H. Kurinami, M. Aoki, T. Ogihara, Y. Kaneda, R. Morishita, Development of efficient plasmid DNA transfer into adult rat central nervous system using microbubble-enhanced ultrasound, Gene Ther. 11 (2004) 1532–1539.

[60] M. Takahashi, K. Kido, A. Aoi, H. Furukawa, M. Ono, T. Kodama, Spinal gene transfer using ultrasound and microbubbles, J. Control. Release 117 (2007) 267–272.

[61] A. Aoi, Y. Watanabe, S. Mori, M. Takahashi, G. Vassaux, T. Kodama, Herpes simplex virus thymidine kinase-mediated suicide gene therapy using nano/microbubbles and ultrasound, Ultrasound Med. Biol. 34 (2008) 425–434.

[62] E. Fattal, G. Barratt, Nanotechnologies and controlled release systems for the delivery of antisense oligonucleotides and small interfering RNA, Br. J. Pharmacol. 157 (2009) 179–194.

[63] S. Kimura, K. Egashira, L. Chen, K. Nakano, E. Iwata, M. Miyagawa, H. Tsujimoto, K. Hara, R. Morishita, K. Sueishi, R. Tominaga, K. Sunagawa, Nanoparticle-mediated delivery of nuclear factor kappaB decoy into lungs ameliorates monocrotaline-induced pulmonary arterial hypertension, Hypertension 53 (2009) 877–883.

[64] K. Tiemann, J.J. Rossi, RNAi-based therapeutics-current status, challenges and prospects EMBO, Mol. Med. 1 (2009) 142–151.

[65] R.E. Vandenbroucke, I. Lentacker, J. Demeester, S.C. De Smedt, N.N. Sanders, Ultrasound assisted siRNA delivery using PEG-siPlex loaded microbubbles, J. Control. Release 126 (2008) 265–273.

[66] C.H. Miao, A.A. Brayman, K.R. Loeb, P. Ye, L. Zhou, P. Mourad, L.A. Crum, Ultrasound enhances gene delivery of human factor IX plasmid, Hum. Gene Ther. 16 (2005) 893–905.

[67] S. Chen, J.H. Ding, R. Bekeredjian, B.Z. Yang, R.V. Shohet, S.A. Johnston, H.E. Hohmeier, C.B. Newgard, P.A. Grayburn, Efficient gene delivery to pancreatic islets with ultrasonic microbubble destruction technology, Proc. Natl. Acad. Sci. U. S. A. 103 (2006) 8469–8474.

[68] Z.P. Shen, A.A. Brayman, L. Chen, C.H. Miao, Ultrasound with microbubbles enhances gene expression of plasmid DNA in the liver via intraportal delivery, Gene Ther. 15 (2008) 1147–1155.

[69] R. Chai, S. Chen, J. Ding, P.A. Grayburn, Efficient, glucose responsive and islet-specific transgene expression by a modified rat insulin promoter, Gene Ther. 16 (2009) 1202–1209.

[70] F.S. Villanueva, R.J. Jankowski, S. Klibanov, M.L. Pina, S.M. Alber, S.C. Watkins, G.H. Brandenburger, W.R. Wagner, Microbubbles targeted to intercellular adhesion molecule-1 bind to activated coronary artery endothelial cells, Circulation 98 (1998) 1–5.

[71] G.E. Weller, E. Lu, M.M. Csikari, A.L. Klibanov, D. Fischer, W.R. Wagner, F.S. Villanueva, Ultrasound imaging of acute cardiac transplant rejection with microbubbles targeted to intercellular adhesion molecule-1, Circulation 108 (2003) 218–224.

[72] D.B. Ellegala, H. Leong-Poi, J.E. Carpenter, A.L. Klibanov, S. Kaul, M.E. Shaffrey, J. Sklenar, J.R. Lindner, Imaging tumor angiogenesis with contrast ultrasound and microbubbles targeted to alpha(v)beta3, Circulation 108 (2003) 336–341.

[73] P. Hauff, M. Reinhardt, A. Briel, N. Debus, M. Schirner, Molecular targeting of lymph nodes with L-selectin ligand-specific US contrast agent: a feasibility study in mice and dogs, Radiology 231 (2004) 667–673.

[74] P.A. Schumann, J.P. Christiansen, R.M. Quigley, T.P. McCreery, R.H. Sweitzer, E.C. Unger, J.R. Lindner, T.O. Matsunaga, Targeted-microbubble binding selectively to GPIIb IIIa receptors of platelet thrombi, Invest. Radiol. 37 (2002) 587–593.

[75] G.E. Weller, F.S. Villanueva, E.M. Tom, W.R. Wagner, Targeted ultrasound contrast agents: in vitro assessment of endothelial dysfunction and multi-targeting to ICAM-1 and sialyl Lewisx, Biotechnol. Bioeng. 92 (2005) 780–788.

[76] C.Z. Behm, B.A. Kaufmann, C. Carr, M. Lankford, J.M. Sanders, C.E. Rose, S. Kaul, J.R. Lindner, Molecular imaging of endothelial vascular cell adhesion molecule-1 expression and inflammatory cell recruitment during vasculogenesis and ischemia-mediated arteriogenesis, Circulation 117 (2008) 2902–2911.

[77] J.R. Lindner, Detection of inflamed plaques with contrast ultrasound, Am. J. Cardiol. 90 (2002) 32L–35L.

[78] K. Hagisawa, N.T., K. Iida, H. Luo, R.J. Siegel, Thrombolysis using low frequency ultrasound with activated platelet targeting bubble liposome in a rabbit iliac artery, Circulation 112 (Sup.II) (2005) 503.

doi:10.1246/cl.2011.298
Published on the web February 16, 2011

Ultrasound-mediated Transfection with Liposomal Bubbles Delivers Plasmid DNA Directly into Nucleus

Takeshi Kawazu,[1] Kazumi Hakamada,[2] Yusuke Oda,[3] Jun Miyake,[2] Kazuo Maruyama,[3] and Takeshi Nagasaki*[1]
[1]*Department of Applied Chemistry and Bioengineering, Graduate School of Engineering, Osaka City University, 3-3-138 Sumiyoshi-ku, Osaka 558-8585*
[2]*Department of Mechanical Science and Bioengineering, Graduate School of Engineering Science, Osaka University, 1-3 Machikaneyama, Toyonaka, Osaka 560-8531*
[3]*Department of Biopharmaceutics, School of Pharmaceutical Sciences, Teikyo University, 1091-1 Suwarashi, Sagamiko, Sagamihara, Kanagawa 229-0195*

(Received January 5, 2011; CL-110002; E-mail: nagasaki@bioa.eng.osaka-cu.ac.jp)

Transfection using ultrasound exposure in the presence of nanobubbles can overcome an important barrier for nonviral gene delivery, that is entering the nucleus without cell division. The monitoring of the relationship between fluorescent protein expression and cell division reveals that ultrasound-mediated transfection with liposomal bubbles is independent on the disappearance of nuclear membrane at mitosis.

In many cases, nonviral gene transfer depends on the cell cycle.[1] Giorgio et al. found that mitosis enhances transgene expression of plasmid DNA delivered by cationic liposomes.[2] The critical rate-determining step for nonviral gene delivery is nuclear entry of an exogenous gene.[3] Although enormous efforts have been directed to this problem, an estimation method has not been established for a long time.[4] Recently Hakamada, Miyake, and co-worker reported the examination of cell morphology and the dynamics of EGFP gene expression by using a fluorescent microscopic apparatus capable of monitoring single cell behavior.[5] With a lipoplex (Lipofectamine LTX, Invitrogen, Carlsbad, CA, USA) as nonviral vector, their results definitely showed that the onset timing of gene expression depended on cell division. This work semiquantitatively demonstrates for the first time that the nuclear envelope determines the rate of nonviral gene delivery.

On the other hand, it is well known that physical methods such as electroporation and sonoporation are effective gene-delivery methods especially for primary cells.[6] Wagner et al. reported that gene transfer by electroporation shows hardly any cell cycle dependence.[7] Maruyama et al. succeeded in the enhancement of sonoporation transfection efficiency by combining ultrasound and acoustic liposomes (bubble liposomes) which contain the ultrasound imaging gas perfluoropropane.[8] Bubble liposomes could act as an effective gene-delivery tool not only in vitro but also in vivo.[9] Under ultrasound exposure, the cavitation of nanobubbles in liposomes induced mechanical constraints on the plasma membrane and increased the membrane permeability by the creation of nanosize pores. The kinetics of protein expression was significantly faster for sonoporation than for lipofection that requires endocytosis.[10] However, very little is known whether ultrasound affects plasmid entry into the nucleus. In this paper, cell division and protein expression kinetics on ultrasound-mediated gene delivery with bubble liposomes have been studied by Hakamada's method.[5]

In 24-well culture plate, NIH3T3 cells (mouse fibroblast) were seeded at 6×10^4 cells per well and cultured at 37 °C with 5% CO_2 atmosphere in 10% FBS-containing DMEM. Cells were transfected with pCMV-Venus encoding a green fluorescent protein (venus) under the control of the CMV promoter. After transfection, phase-contrast and fluorescent images of cells in each well were recorded at intervals of 10 min for 30 h, and their exposure times were 50 and 400 ms, respectively. The measurement was started at 1 h post-transfection. As a compared nonviral gene carrier, linear poly(ethyleneimine)s (jetPEI, Polyplus-Transfection, Illkirch, France) was used because it showed high transfection ability in vitro and in vivo.[11] The transfection procedure was followed with manufacturer's instruction. On the other hand, preparation of bubble liposomes and transfection of plasmid DNA using bubble liposomes are carried out according to similar way previously reported by Maruyama et al.[8b] The ultrasound was exposed for 10 s under following conditions: frequency, 2 MHz, duty, 50%; intensity, 2.5 W cm^{-2}; burst rate, 2 Hz using Sonopore 3000 (NEPA GENE, CO., LTD., Chiba, Japan).

The results of jetPEI (Figure 1a) show a similar relationship between the timing of cell division and the onset timing of gene expression as that by lipofection.[5] The peak of protein expressing cells appeared around 10 h post-transfection

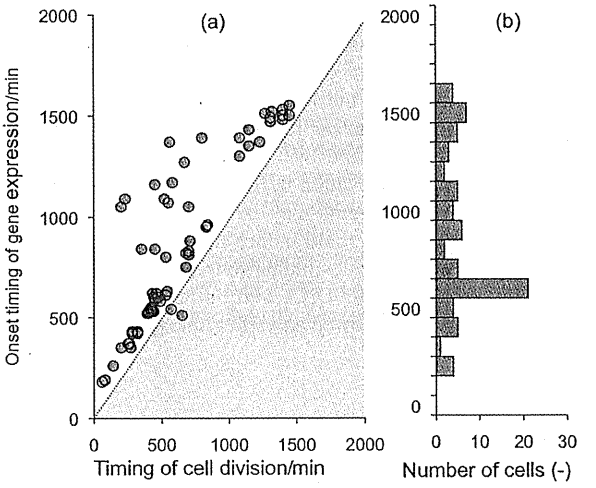

Figure 1. (a) Correlation between the timing of cell division and the onset of protein expression by jetPEI-mediated transfection. (b) Distribution of the cell number on the onset timing on jetPEI-mediated transfection.

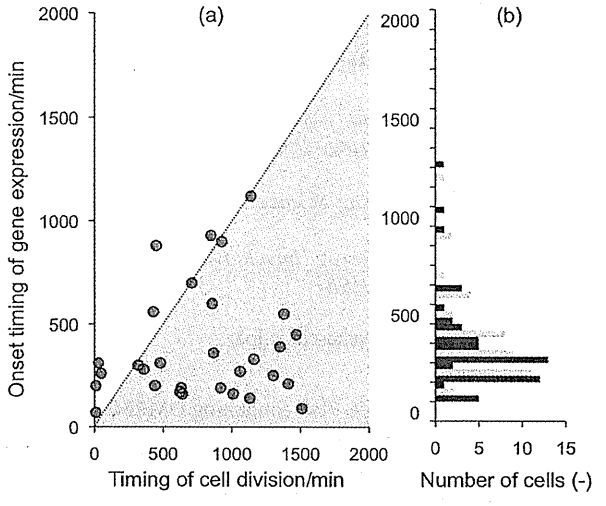

Figure 2. (a) Correlation between the timing of cell division and the onset of protein expression on ultrasound-mediated transfection with bubble liposomes. (b) Distribution of the cell number on the onset timing on ultrasound-mediated transfection with bubble liposomes; expressing after division (blue), expressing before division (yellow), expressing without division (red), respectively.

(Figure 1b). The polymeric nonviral gene transfection obviously depended on cell division although Wagner et al. mentioned cell-cycle-independent gene transfection by linear PEI.[7]

On the contrary, correlation between the timing of cell division and the onset of protein expression by ultrasound-mediated transfection in the presence of liposomal bubbles is shown in Figure 2. Under these conditions, sonoporation did not show cytotoxicity at all by WST assay. There is no relationship between the timing of cell division and the onset of protein expression. Before 10 h post-transfection, more than 80% of cells expressed the protein without cell division unlike jet-PEI (Figure 2b). The kinetics of gene expression showed that ultrasound-mediated transfection with nanobubbles allowed a rapid and direct transfer of naked DNA not only into the cytoplasm but also into the nucleus, probably via ultrasound-induced pores in the nuclear membrane. The transient perforation of plasma membrane by collapse of microbubbles was confirmed by SEM observation by Kudo et al.[12] The maximum velocity of the microstreams may be 700 m s^{-1}.[13] These rapid and strong microstreams could induce transient pores at plasma and nuclear membranes simultaneously and enhance the permeability of exogenous DNA into the nucleus. The expression after cell division showed an earlier time profile than that of jet-PEI; that also suggests direct transfer of plasmid DNA into cytoplasm rather than endocytosis.

In summary, our results demonstrate that ultrasound-mediated gene transfer with liposomal bubbles is nontoxic and effective under appropriate conditions even toward nondividing cells. We expect these findings will enhance the utility of current sonoporation, particularly in gene and drug delivery.

References

1 S. Brunner, T. Sauer, S. Carotta, M. Cotton, M. Saltik, E. Wagner, *Gene Ther.* **2000**, *7*, 401.
2 W. C. Tseng, F. R. Haselton, T. D. Giorgio, *Biochim. Biophys. Acta, Gene Struct. Expression* **1999**, *1445*, 53.
3 M. E. Dowty, P. Williams, G. Zhang, J. E. Hagstrom, J. A. Wolff, *Proc. Natl. Acad. Sci. U.S.A.* **1995**, *92*, 4572; J. J. Ludtke, M. G. Sebestyen, A. Wolff, *Mol. Ther.* **2002**, *5*, 579; C. W. Pouton, K. M. Wagstaff, D. M. Roth, G. W. Mosley, D. A. Jans, *Adv. Drug Delivery Rev.* **2007**, *59*, 698.
4 T. Nagasaki, T. Kawazu, T. Tachibana, S. Tamagaki, S. Shinkai, *J. Controlled Release* **2005**, *103*, 199; T. Masuda, H. Akita, T. Nishio, K. Niikura, K. Kogure, K. Ijiro, H. Harashima, *Biomaterials* **2008**, *29*, 709; A. P. Lam, D. A. Dean, *Gene Ther.* **2010**, *17*, 439.
5 K. Hakamada, S. Fujita, J. Miyake, *J. Biosci. Bioeng.* **2010**, *109*, 62.
6 M. Duvshani-Eshet, L. Baruch, E. Kesselman, E. Shimoni, M. Machluf, *Gene Ther.* **2006**, *13*, 163; J. M. Escoffre, J. Teissié, M. P. Rols, *J. Membr. Biol.* **2010**, *236*, 61.
7 S. Brunner, E. Fürtbauer, T. Sauer, M. Kursa, E. Wagner, *Mol. Ther.* **2002**, *5*, 80.
8 a) R. Suzuki, T. Takizawa, Y. Negishi, N. Utoguchi, K. Maruyama, *J. Drug Targeting* **2007**, *15*, 531. b) R. Suzuki, T. Takizawa, Y. Negishi, K. Hagisawa, K. Tanaka, K. Sawamura, N. Utoguchi, T. Nishioka, K. Maruyama, *J. Controlled Release* **2007**, *117*, 130.
9 R. Suzuki, T. Takizawa, Y. Negishi, N. Utoguchi, K. Sawamura, K. Tanaka, E. Namai, Y. Oda, Y. Matsumura, K. Maruyama, *J. Controlled Release* **2008**, *125*, 137; R. Suzuki, E. Namai, Y. Oda, N. Nishiie, S. Otake, R. Koshima, K. Hirata, Y. Taira, N. Utoguchi, Y. Negishi, S. Nakagawa, K. Maruyama, *J. Controlled Release* **2010**, *142*, 245.
10 S. Mehier-Humbert, T. Bettinger, F. Yan, R. H. Guy, *J. Controlled Release* **2005**, *104*, 203.
11 O. Boussif, F. Lezoualc'h, M. A. Zanta, M. D. Mergny, D. Scherman, B. Demeneix, J. P. Behr, *Proc. Natl. Acad. Sci. U.S.A.* **1995**, *92*, 7297.
12 N. Kudo, K. Okada, K. Yamamoto, *Biophys. J.* **2009**, *96*, 4866.
13 S. Hernot, A. L. Klibanov, *Adv. Drug Delivery Rev.* **2008**, *60*, 1153.

Ultrasonics Sonochemistry 18 (2011) 425–430

Contents lists available at ScienceDirect

Ultrasonics Sonochemistry

journal homepage: www.elsevier.com/locate/ultsonch

Synergistic effect of ultrasound and antibiotics against *Chlamydia trachomatis*-infected human epithelial cells in vitro

Yurika Ikeda-Dantsuji [a], Loreto B. Feril Jr. [a,*], Katsuro Tachibana [a], Koichi Ogawa [a], Hitomi Endo [a], Yoshimi Harada [a], Ryo Suzuki [b], Kazuo Maruyama [b]

[a] Department of Anatomy, Fukuoka University School of Medicine, Fukuoka, Japan
[b] Department of Biopharmaceutics, School of Pharmaceutical Sciences, Teikyo University, Kanagawa, Japan

ARTICLE INFO

Article history:
Received 12 April 2010
Received in revised form 12 July 2010
Accepted 21 July 2010
Available online 27 July 2010

Keywords:
Ultrasound
Nanobubbles
Antibiotic
Intracellular bacteria

ABSTRACT

To investigate whether or not the combined ultrasound and antibiotic treatment is effective against chlamydial infection, a new ultrasound exposure system was designed to treat chlamydia-infected cells. First, the minimum inhibitory concentrations of antibiotics against *Chlamydia trachomatis* were determined. Infected cultures were treated with antibiotics then sonicated at intensity of 0.15 or 0.44 W/cm^2 with or without Bubble liposomes. After 48 or 72 h after infection, chlamydial inclusions were stained and examined by fluorescence microscopy. The internalization of dextran–fluorescein conjugates by ultrasound irradiation with Bubble liposomes was observed by fluorescence microscopy. The results showed that application of nanobubble-enhanced ultrasound caused no significant effect on cell viability and chlamydial infectivity. However, Doxycycline (1/2 MIC) or CZX (1.0 μg/ml) in combination with nanobubble-enhanced ultrasound dramatically reduced the number of inclusions compared with that administered with antibiotics only. Bubble dose-dependent synergy was also observed. After ultrasound irradiation at intensity of 0.44 W/cm^2 on the presence of Bubble liposomes, 10% of HeLa cells were observed to have internalized the dextran molecules. This study suggests the possibility of using nanobubble-enhanced ultrasound to deliver antibiotic molecules into cells to eradiate intracellular bacteria, such as chlamydiae, without causing much damage to the cells itself.

1. Introduction

An obligate intracellular pathogen, *Chlamydia trachomatis*, is the most prevalent sexually transmitted bacterium worldwide [1]. *C. trachomatis* is a Gram-negative bacterium which has a unique biphasic developmental cycle characterized by an infectious but metabolically inactive extracellular form, called the 'elementary body', which initiates infection through the uptake by the host cell. Thereafter, elementary bodies differentiate into noninfectious but metabolically active forms, called the 'reticulate body', which proliferate within the inclusion. Reticulate bodies also differentiate back to elementary bodies before release at the end of the developmental cycle. At its sites of primary infection, *C. trachomatis* infects the urethral or cervical epithelium, causing acute urethritis or cervicitis [2]. These frequently progress into chronic inflammatory disease, the most significant of which, is chronic salpingitis, an inflammatory disease of fallopian tubes that can result in pelvic inflammatory disease, ectopic pregnancy, and tubal infertility [3].

The recommended antibiotic treatments for urogenital infections are a single dose of azithromycin or a 7-day course of doxycycline for management of active infections [4]. These regimens have been shown to result in satisfactory cure rates of acute infections [5,6]; however, chronic diseases (designated "persistent infection") have been suggested to be less responsive to antibiotic therapy [7].

Previous work has shown that some antibiotics treatment of *Pseudomonas aeruginosa* or *Escherichia coli* coupled with ultrasound irradiation enhances the bactericidal activity [8]. The more recent research has revealed that similar synergistic effects of combined ultrasound and antibiotic treatment are seen in both Gram-positive and Gram-negative bacteria with some antibiotics, especially the aminoglycosides [9]. It is not clear whether the combined ultrasound and antibiotic treatment are effective on intracellular pathogen, e.g. chlamydial infection. If an intracellular bacterial infection could be efficiently eradicated from an infected person, one could avoid chronic antibiotic treatments. In addition, this strategy of treatment could be beneficial in the management of chlamydial persistent diseases.

Here, we are studying the synergistic use of ultrasound and antibiotics to kill the *chlamydia*. This report presents results of

* Corresponding author. Address: 7-45-1 Nanakuma, Jonan-ku, Fukuoka 814-0180 Japan. Tel.: +81 92 801 1011x3206; fax: +81 92 865 6032.
E-mail addresses: ferilism@yahoo.com, feril@fukuoka-u.ac.jp (L.B. Feril).

1350-4177/$ - see front matter © 2010 Elsevier B.V. All rights reserved.
doi:10.1016/j.ultsonch.2010.07.015

the first step in that research, which is investigation of the in vitro response of *C. trachomatis*-infected human epithelial cells to combination of ultrasound and two types of antibiotics.

2. Materials and methods

2.1. Chlamydial strain and cell lines

C. trachomatis serovar E/UW-5/Cx was prepared in McCoy cells and propagated according to a previously reported method [10]. The mouse fibroblast cell line McCoy cell (CRL 1696) and human epithelial cell line HeLa 229 cell (CLL 2.1) were maintained in Dulbecco's modified Eagle medium (DMEM, Invitrogen, Grand Island, NY, USA) supplemented with 10% heat-inactivated fetal calf serum (FCS, Invitrogen) and 100 μg/ml streptomycin.

2.2. Infection of HeLa cells

The HeLa cells were seeded into a 24-well plate with lumox™ fluorocarbon film base (optically clear, 50 μm-thin, gas permeable film, Greiner bio-one, Gottingen, Germany). Stocks of chlamydial strain were diluted with sucrose–phosphate–glutamate (SPG) medium [10]. Chlamydial suspensions of 0.5×10^4 inclusion-forming units (IFUs) in 0.25 ml SPG medium were inoculated onto the monolayer cultures of HeLa cells (1×10^4 cells/well). This is equivalent to a multiplicity of infection of 0.5. After incubation at 37 °C for 90 min, the inoculum was decanted, and the cells were washed in medium to remove the nonadsorbed chlamydiae and were then further incubated in 1 ml DMEM containing 1 μg/ml cycloheximide (Sigma Chemicals, St. Louis, MO, USA) and 2% FCS (maintenance medium).

2.3. Preparation of bubble liposome

Bubble liposomes were prepared according to a method previously described [11]. Liposomes composed of 1,2-distearoyl-sn-glycero-phosphatidylcholine (DSPC) (NOF Corp., Tokyo, Japan) and 1,2-distearoyl-snglycero-3-phosphatidyl-ethanolamine-methoxypolyethyleneglycol(DSPE-PEG(2k)-OMe, (PEG Mw = ca. 2000), NOF) (94: 6 (m/m)) were prepared by reverse phase evaporation. Briefly, all reagents (totallipid: 100 μmol) were dissolved in 8 ml of 1:1 (v/v) chloroform/diisopropyl ether, then 4 ml of phosphate buffered saline (PBS) were added. The mixture was sonicated and evaporated at 65 °C. The solvent was completely removed, and the size of the liposomes was adjusted to less than 200 nm using an extruding apparatus (Northern Lipids Inc., Vancouver, BC, Canada) and sizing filters (pore sizes: 100 and 200 nm; Nuclepore Track-Etch Membrane, Whatman plc, UK). After sizing, the liposomes were sterilized by passing them through a 0.45 μm pore size filter (MILLEX HV filter unit, Durapore PVDF membrane, Millipore Corp., MA, USA). The size of the liposomes was measured by dynamic light scattering (ELS-800, Otsuka Electronics Co., Ltd., Osaka, Japan). The average diameter of these liposomes was between 150 and 200 nm. Lipid concentration was measured using the Phospholipid C test (Wako Pure Chemical Industries). BLs were prepared from the liposomes and perfluoropropane gas (Takachiho Chemical Industrial Co., Ltd., Tokyo, Japan). Briefly, 5 ml sterilized vials containing 2 ml of the liposome suspension (lipid concentration: 2 mg/ml) were filled with perfluoropropane, capped, and then supercharged with 7.5 ml of perfluoropropane. The vial was placed in a bath-type sonicator (42 kHz, 100 W; BRANSONIC 2510J-DTH, Branson Ultrasonics Co., Danbury, CT, USA) for 5 min to form the BLs. In this method, the liposomes were reconstituted by sonication under the condition of supercharge with perfluoropropane in the 5 ml vial container. At the same time, perfluoropropane would be entrapped within lipids like micelles, which were made by DSPC and DSPE-PEG(2k)-OMe from liposome composition, to form nanobubbles. The lipid nanobubbles were encapsulated within the reconstituted liposomes, which sizes were changed into around 1 μm from 150 to 200 nm of original.

2.4. Immunofluorescence staining and fluorescence microscopy

At 48 or 72 h after infection, the infected monolayers were washed with PBS, and the cells were fixed with −20 °C chilled methanol. After the specimens had been dried, the inclusion bodies were stained with fluorescein isothiocyanate (FITC)-labeled monoclonal antibody against *C. trachomatis* lipopolysaccharides (Progen Biotechnik, Heidelberg, Germany) for 30 min at room temperature. The cells were rinsed with saline, and the films were cut off from the plate, and mounted in a 1:1 solution of PBS–glycerol. The antibody staining resulted in yellow–green chlamydial proteins, and Evans blue counterstaining yielded red eukaryotic cells. The formation of inclusions was assessed using a Zeiss Axiophot fluorescence microscope. The cells positive for inclusions are considered infected cells and infectivity was presented as the number of inclusion-forming units (IFUs).

2.5. Antibiotics and measurements of MICs

Doxycycline (DOX, Sigma Chemicals) and ceftizoxime (CZX, Fujisawa Yakuhin Kogyou, Tokyo, Japan) were obtained in powder form. Both antibiotics were diluted with saline, and were dissolved in maintenance medium at a concentration of 100 μg/ml and frozen at −80 °C until used. The minimum inhibitory concentrations (MICs) were determined using a method previously described [12]. Briefly, confluent monolayer cultures of cells in a 24-well flat-bottomed plate with 13-mm coverslips were inoculated by centrifugation and incubated in 1 ml of maintenance medium containing a serial dilution of antibiotics for 72 h. To determine the MICs, the cover slips were stained and observed as described in Immunofluorescence staining and fluorescence microscopy. The lowest concentration of the antimicrobial agent that completely inhibited the formation of visible chlamydial inclusions was determined as the MIC.

2.6. Ultrasound exposure

An acoustically transparent gel (Pharmaceutical Innovations Inc., Newark, NJ) was applied on the ultrasound probe before positioning the plate containing the sample on top of it (Fig. 1). Thera-

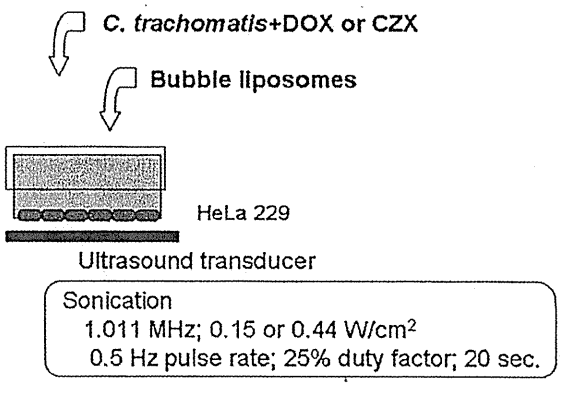

Fig. 1. Experimental design. Schematic drawing of the ultrasound setting. *C. trachomatis*-infected HeLa cells were exposed to ultrasound after addition of antibiotic and Bubble liposomes.

peutic ultrasound (1.011 MHz) was irradiated from a device (Sono-Pore KTAC-4000, NepaGene, Chiba, Japan) at intensity of 0.15 or 0.44 W/cm^2 (duty cycle of 25%) for 20 s immediately after addition of Bubble liposomes into the sample.

2.7. Measurement of cell viability

The Trypan blue dye exclusion test was carried out by mixing 200 μl of the suspension of HeLa cells with an equal amount of 0.3% Trypan blue solution (Sigma Chemicals) in PBS. After 5 min incubation at room temperature, the number of cells excluding Trypan blue was counted using a C-Chip disposable hemocytometer (Digital Bio Technology Co., Gyeonggi, Korea) to estimate the number of viable cells immediately after sonication.

2.8. Measurement of infectivity of chlamydiae

The 1.0 ml of chlamydial suspensions in SPG treated with ultrasound and/or nanobubbles was inoculated into triplicate cultures of McCoy cells in order to estimate the infectivity immediately after sonication. Chlamydial suspensions, 0.25 ml each, were added onto the monolayer culture of McCoy cells. After centrifugation at 1000g for 60 min, the inoculum was decanted, and the cells were washed with medium to remove the nonadsorbed chlamydiae, and were then further incubated in 1.0 ml of maintenance medium.

2.9. Internalization of dextran–fluorescein conjugates

Dextran–fluorescein conjugates (3000 MW, anionic: Molecular Probes, Inc., OR, USA) were soluble in 0.02 M Tris–HCl buffer (pH 8.0) at 10 μg/ml, and performed by filtration using 0.2 μm pore-diameter sterile filters. Aqueous solutions of dextran were diluted to 10 μg/ml with maintenance medium. The 50 μl of solution of dextran conjugates instead of antibiotics were added into the monolayer cultures of HeLa cells in a 24-well plate with lumox™ fluorocarbon film bottom. Ultrasound was irradiated for 20 s with or without Bubble liposomes at 50 μg/ml. Cultures were rinsed in PBS(−) solution and examined immediately after rinsing by fluorescent microscopy (Leica Microsystems CTR4000, Wetzlar, Germany).

2.10. Statistical analysis

Data from these study were analyzed using unpaired *t*-test including Welch's correction. Results were considered to be significant when the corrected *p*-value is less than 0.05, indicated as $p < 0.05$ in the manuscript and figure legends. Error bars shown in the figures are standard deviations of duplicate samples in experiments repeated at least three times.

3. Results

3.1. Cell viability of HeLa cells and infectivity of chlamydiae by nanobubble-enhanced ultrasound

We first investigated whether nanobubble-enhanced ultrasound decreased the cell viability of HeLa cells and the infectivity of chlamydia. As shown in Table 1, ultrasound at intensity of 0.44 W/cm^2 caused no significant effect, but ultrasound at intensity of 0.15 W/cm^2 decreased slightly on cell viability. On the other hand, the application of ultrasound also caused no significant effect on chlamydial infectivity at both intensities of 0.15 and 0.44 W/cm^2 (Fig. 2).

Table 1
Viable cell counts following exposure of HeLa cell to ultrasound.

Application of ultrasound	Cytotoxicity: No. of viable cells/well (% of control)
Control	
(−) Sonication	7475 ± 1950
(−) Bubble liposomes	(100)
Bubble	
(−) Sonication	8940 ± 950
(+) Bubble liposomes	(120)
Ultrasound (0.15 W/cm^2)	6290 ± 950
(+) Bubble liposomes	(84)
Ultrasound (0.44 W/cm^2)	7865 ± 950
(+) Bubble liposomes	(105)

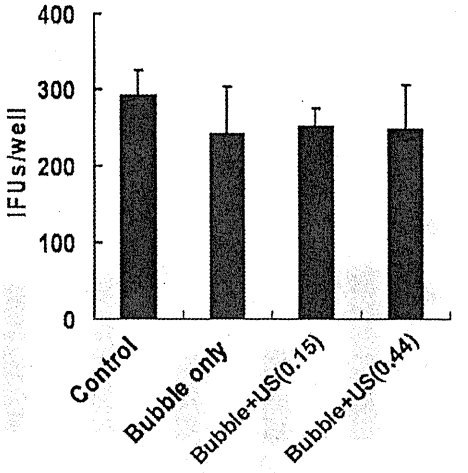

Fig. 2. Infectivity of chlamydiae by nanobubble-enhanced ultrasound. No significant change in infectivity when cells were treated with bubble liposomes (Bubble only) or ultrasound at intensities 0.15 W/cm^2 (Bubble + US(0.15)) and 0.44 W/cm^2 (Bubble + US(0.44)) in the presence of bubble liposomes.

3.2. Ultrasonic enhancement of antibiotic action on C. trachomatis-infected HeLa cells

The MIC of DOX for *C. trachomatis*-infected HeLa cells was determined to be 0.03 μg/ml. Infected cultures were treated with DOX at 1/2 MIC (0.015 μg/ml) then sonicated with or without the addition of Bubble liposomes (50 μg/ml). The results showed that ultrasound alone or Bubble liposomes alone did not decrease the formation of inclusions in infected cells administered with DOX (Fig. 3). However, DOX at 1/2 MIC in combination with nanobubble-enhanced ultrasound significantly reduced the number of IFUs to 66 ± 39% and 15 ± 12%, respectively, at intensities of 0.15 and 0.44 W/cm^2, compared with that administered with DOX at 1/2 MIC only (Control in Fig. 3).

The MIC of CZX for *C. trachomatis*-infected HeLa cells could not be determined because intracellular pathogens are known to be resistant to CZX, therefore, we tried to use considerably high concentrations of 0.125, 0.25, 0.5 and 1.0 μg/ml. Any of the concentrations used did not show any effect against chlamydia when applied alone but in combination with bubble-enhanced ultrasound, significant IFU reduction was observed and most with 1.0 μg/ml CZX (data not shown). Similar to the observed effect with DOX, 1.0 μg/ml CZX in combination with nanobubble-enhanced ultrasound also reduced the number of IFUs to 53 ± 32% and 50 ± 48%, respectively, at intensities of 0.15 and 0.44 W/cm^2, compared with that administered 1.0 μg/ml CZX only (Fig. 4).

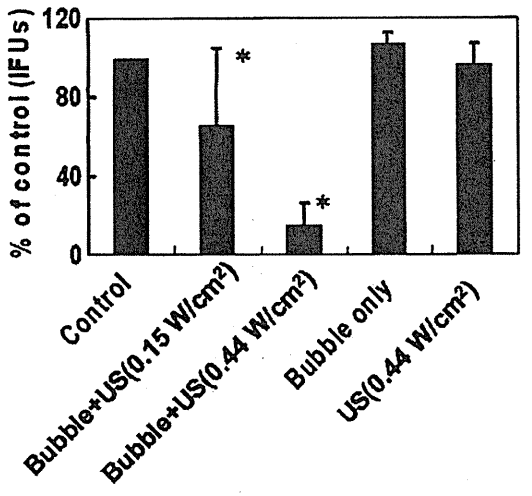

Fig. 3. Ultrasonic enhancement of bactericidal activity of doxycycline (DOX) at 1/2 MIC on *C. trachomatis*-infected HeLa cells. Data represents % of control that is the number of chlamydial inclusions treated with DOX at 1/2 MIC only (*$p < 0.05$).

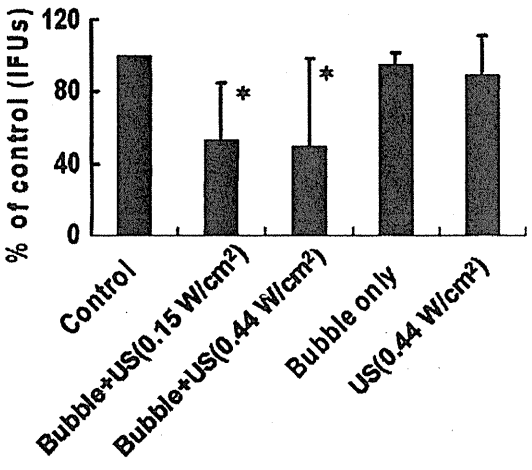

Fig. 4. Ultrasonic enhancement of bactericidal activity of ceftizoxime (CZX) at 1.0 μg/ml on *C. trachomatis*-infected HeLa cells. Data represents % of control that is the number of chlamydial inclusions treated with CZX at 1.0 μg/ml only (*$p < 0.05$).

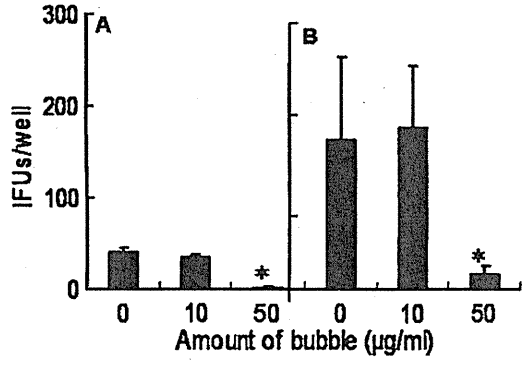

Fig. 5. Effect of concentration of Bubble liposomes in addition with ultrasound irradiation and antibiotics on *C. trachomatis*-infected HeLa cells. (A) Before ultrasound irradiation, the infected culture was treated with DOX at 1/2 MIC. (B) Before ultrasound irradiation, the infected culture was treated with CZX at 1.0 μg/ml (*$p < 0.05$).

Next, we examined the effect of the amount of Bubble liposomes on nanobubble-enhanced ultrasound reduction of IFU. With increased amount of Bubble liposomes, the synergistic effect of ultrasound and DOX was significantly increased (Fig. 5A). Bubble dose-dependent synergy was also observed with CZX and ultrasound (Fig. 5B).

3.3. Internalization of dextran–fluorescein conjugates by ultrasound

Finally, to examine whether ultrasound can facilitate intracellular uptake of large molecules, we sonicated HeLa cells in the presence of fluorescein-labeled dextran and afterwards examined the cells by fluorescence microscopy. Approximately 10% of viable cells were observed to have internalized the dextran molecules after ultrasound irradiation at intensity of 0.44 W/cm^2 in the presence of Bubble liposomes (Fig. 6). This observation showed that ultrasound can facilitate cellular uptake of large molecules.

4. Discussion

Previous reports have shown a synergistic effect between ultrasound and antibiotics in killing *E. coli* and *P. aeruginosa* [8]. The purpose of this present study was to determine if the same synergistic effect could be observed with *C. trachomatis* even if this is an intracellular organism. The results of the MIC experiments and the measurements of bactericidal activity against *C. trachomatis* show that addition of nanobubble-enhanced ultrasound to DOX treatment enhanced the effectiveness of DOX in eradicating *C. trachomatis* (Fig. 3). Dramatic reduction of IFUs to 15 ± 12% was observed at higher ultrasound intensity of 0.44 W/cm^2 (Fig. 3). These findings could have important clinical applications because the tissue concentration of antibiotics often became below the MICs in actual clinical settings.

In a previous study, the duration of the illness in patients with *C. trachomatis*-triggered reactive arthritis (ReA) was shorter in patients treated with lymecycline for 3 months than in a placebo-treated group [13]. Other studies on the long-term treatment of acute ReA with ciprofloxacin showed no advantage over placebo treatment in the outcome of ReA [14]. So far, the optimal treatment of ReA with antimicrobial drugs remains controversial. In addition, it was recently reported that persistent chlamydial infection induced ReA [15–17]. Most recent finding by Reveneau et al. have shown that persistent chlamydial forms are more resistant to DOX than acute forms because of the decreased antibiotic uptake by host cells [18]. Therefore, a more effective treatment of persistent chlamydial infections requires a method to increase antibiotics uptake by the infected cells. On the other hand, advances in ultrasound and nanobubble-enhanced ultrasound technologies have raised the possibility of using ultrasound not only for diagnostic but also for therapeutic purposes. The combination of an agent as nanobubbles and ultrasound exposure makes sonoporation possible. Sonoporation is characterized by a transient change in cellular membrane permeability mediated by ultrasound [19–24]; the cavitation energy created by the bubble collapse is thought to be the key mechanism [19]. Thereby, we confirmed that the intracellular delivery of macromolecules such as dextran was observed under the condition used in our experiments (Fig. 6). In addition, ultrasound did not damage HeLa cells or chlamydial organisms in the presence of Bubble liposomes (Fig. 2 and Table 1). This may be due to the size of the bubbles such that cavitations created are enough to deliver the drug to the cells but not "large" enough to create fatal damage to the cell itself. However, to understand the dynamic of the interactions between nanobubble, cell membrane and ultrasound [25], further study is needed. Collectively, our data suggest the possibility of using nanobubble-en-